Aerospace Science and Technology 168 (2026) 111217

Contents lists available at ScienceDirect

Aerospace Science and Technology

journal homepage: www.elsevier.com/locate/aescte

Collision-Free Robust Trajectory Tracking Control for Fixed-Wing UAV with Flexible Performance Constraints

Chao Yan [a], Zexu Zhang [a,*], Weimin Bao [a,b], Kai Zhang [a], Liang Zhang [c]

[a] School of Astronautics, Harbin Institute of Technology, Harbin, 150001, China
[b] China Aerospace Science and Technology Corporation, Beijing, 100048, China
[c] School of Electrical Engineering and Automation, Anhui University, Hefei, 230039, China

ARTICLE INFO

Editor: Chaoyong Li

Keywords:
Fixed-wing UAV
Trajectory tracking
Prescribed performance
Control barrier function
Quadratic programming
Adaptive adjustment signal

ABSTRACT

This paper investigates the safety-critical trajectory tracking for a fixed-wing unmanned aerial vehicle (UAV) considering prescribed performance requirements, unknown disturbances, and both static and dynamic obstacles. First, a class of polynomial performance functions is designed to naturally satisfy the initial condition and achieve quantitative performance requirements. Based on this, a prescribed performance trajectory tracking controller is developed to ensure that the tracking error remains within the performance boundaries. Second, an obstacle avoidance method that couples control barrier function (CBF) theory with a predefined-time disturbance observer is proposed. This method attenuates the effect of disturbances on UAV flight within a predefined time, thereby rigorously ensuring obstacle avoidance safety and improving the disturbance rejection capability. Furthermore, within a quadratic programming framework, the prescribed-performance controller is integrated with CBFs to preserve tracking performance as much as possible while ensuring flight safety. Finally, to address potential violations of the performance boundaries during obstacle avoidance, adaptive adjustment signals are designed based on positive system theory to achieve flexible relaxation of the performance boundaries. Theoretical analysis demonstrates that the proposed scheme guarantees both obstacle avoidance safety and continuous tracking of the desired trajectory, even in the presence of unknown disturbances. Simulations validate the effectiveness and advantages of the proposed method in environments with obstacles and disturbances.

1. Introduction

Fixed-wing unmanned aerial vehicles (UAVs), leveraging their advantages of long endurance, high cruising speed, large payload capacity, and cost-effectiveness, have been widely applied in both civilian and military domains, such as forest fire monitoring [1], formation flight [2], and target search and tracking [3]. In complex environments, UAVs frequently encounter unknown disturbances and obstacles. Consequently, achieving high-performance trajectory tracking while ensuring safety has become an urgent requirement for fixed-wing UAVs to accomplish missions rapidly and effectively. From a performance perspective, the controller is designed to drive the UAV to follow a desired trajectory while satisfying prescribed performance requirements, such as user-specified convergence time and steady-state error. From a safety perspective, it is essential for the UAV to maintain a safe distance from obstacles during trajectory tracking. However, a conflict often arises between trajectory tracking performance and flight safety. Thus, designing a control strategy that effectively balances these two aspects is of significant theoretical and practical importance for fixed-wing UAVs.

For the trajectory tracking problem of fixed-wing UAVs, various advanced feedback control methods were proposed in [4–9]. These approaches primarily focus on the convergence time and stability of the closed-loop system but, to some extent, overlook the transient performance and steady-state accuracy of the tracking error. Recently, prescribed performance control (PPC), pioneered in [10], was shown to ensure that the tracking error evolves within predefined performance boundaries, thereby achieving both transient performance (e.g., overshoot and convergence time) and steady-state accuracy. Due to its advantages in performance constraints, PPC has attracted considerable attention. Recent studies primarily focus on the design of performance functions that characterize performance boundaries for the system. To address the issue of infinite convergence time associated with traditional performance functions [10–13], fixed-time performance functions were

* Corresponding author.
E-mail address: zexuzhang@hit.edu.cn (Z. Zhang).

https://doi.org/10.1016/j.ast.2025.111217
Received 6 September 2025; Received in revised form 15 October 2025; Accepted 2 November 2025
Available online 4 November 2025

developed in [14–17], allowing the convergence time to be specified in advance. Furthermore, to reduce overshoot, enhanced performance functions were proposed in [18–22], effectively constraining the variation range of the tracking error by utilizing a pair of same-side boundaries. However, when the system restarts or the desired state changes, the aforementioned methods [10–22] require redesigning the performance functions and verifying the initial condition. This not only limits the autonomous operation capability of the system but also increases the complexity of controller design. To mitigate this issue, performance functions with large initial values were introduced in [23–25]. Nevertheless, the enlarged performance constraints during the initial phase may compromise transient performance. Performance functions related to the initial tracking error were designed in [26–28], which can automatically adapt to arbitrary known initial condition, but their drawback is the inability to precisely prescribe the convergence time. Therefore, it is necessary to systematically develop a new class of performance functions that naturally satisfy the initial condition while achieving quantitative performance requirements.

In environments with obstacles, the safe flight of UAVs requires maintaining a safe distance from surrounding objects [29]. A straightforward approach is the artificial potential field (APF), which generates a strong repulsive force when the controlled object approaches an obstacle [30,31]. Another method is the control barrier function (CBF), which encodes system safety constraints through the forward invariance of state sets [32–35]. Compared with APF, CBF not only provides provable safety guarantee but also yields smoother control behavior [36]. In practical missions, UAVs inevitably encounter external disturbances [37–39]. Since CBFs heavily rely on precise system models, disturbances may drive the system state beyond the safe set. Input-to-state safe CBFs [40,41] ensure the forward invariance of an enlarged set under disturbances, but fail to guarantee the invariance of the original safe set. Robust CBFs [42–44], typically designed based on worst-case disturbance bounds, ensure safety but may result in an overly conservative admissible safe input set. Recent studies have combined disturbance observers with CBFs to achieve robust safety by actively estimating external disturbances [45–47]. However, these approaches require knowledge of the upper bound of disturbance estimation error. In [48], a Lyapunov function was employed to characterize disturbance estimation error, thereby eliminating the dependence on such an upper bound, but the method is only applicable to specific types of disturbances. Moreover, the aforementioned disturbance observers [45–48] achieve only asymptotic convergence. By contrast, the predefined-time disturbance observer (PTDO) can achieve high-precision disturbance estimation within a predefined time. Therefore, integrating PTDO with CBFs holds the potential to more rapidly suppress the impact of disturbances while ensuring strict robust safety and improving control performance.

The obstacle avoidance process in UAVs can degrade trajectory tracking performance, which in turn leads to an increase in tracking error. However, the performance requirements in PPC remain invariant, which conflicts with the control capability degradation during obstacle avoidance. Singularity issues may arise once the actual error exceeds the prescribed boundaries. In [13,23] and [12,18–20], singularity issues caused by disturbances and input saturation were addressed by introducing modification signals into the performance functions to achieve dynamic relaxation of performance constraints. Nevertheless, these approaches cannot be directly extended to handle singularities arising from obstacle avoidance. Therefore, further investigation is required to effectively address the potential singularities of PPC induced by obstacle avoidance.

Motivated by the above discussion, this paper investigates safe trajectory tracking for a fixed-wing UAV under unknown disturbances and performance constraints. A novel control scheme is proposed, which effectively balances tracking performance and flight safety. The proposed scheme integrates PPC, a PTDO, and CBFs within a unified framework. It elucidates how, when performance requirements conflict with safety constraints, appropriately relaxing tracking performance can ensure that the UAV trajectory remains strictly within the safe region. The main contributions of this paper are summarized as follows:

1. A safety-critical trajectory tracking control strategy is proposed based on quadratic programming (QP) for a fixed-wing UAV operating in complex environments with external disturbances and obstacles. Specifically, a PPC-based controller forms the performance baseline, while CBFs are constructed using a PTDO to serve as safety constraints. These components are unified within the QP framework. The proposed strategy strictly ensures obstacle avoidance safety and accurate trajectory tracking, even in the presence of disturbances. Compared to existing trajectory tracking approaches [4–9,21–23,35], this study simultaneously considers external disturbances, obstacle avoidance, and performance constraints. The investigated problem is more practically significant and challenging due to the potential conflicts between performance objectives and safety constraints, as well as the possibility of safety constraint violations induced by disturbances.
2. Unlike existing performance functions [10–28], this paper designs a class of polynomial performance functions (PPFs) that can pre-quantify overshoot, settling time, and steady-state tracking error accuracy, while naturally satisfying the initial condition. Moreover, nonnegative adaptive adjustment signals are introduced to dynamically quantify the performance degradation caused by obstacle avoidance, and to elastically relax the performance boundaries, thereby effectively avoiding potential singularity issues in PPC.
3. A real-time obstacle avoidance method is proposed by combining a PTDO and CBFs, ensuring that the UAV maintains a safe distance from obstacles even in the presence of unknown disturbances. In contrast to robust CBFs in [42–44], which rely on known disturbance bounds, the proposed method actively estimates and compensates for disturbances via the observer, thereby reducing the conservativeness of the admissible safe control input set. Furthermore, compared to the method in [45–48], the designed PTDO enables faster elimination of the disturbance impact on system safety. Its convergence time is predefined, thereby enhancing the flexibility of system performance.

The remainder of this paper is organized as follows. Section 2 introduces necessary lemmas and the formal problem statement. Section 3 presents the design of a class of PPFs and adaptive adjustment signals. Section 4 first develops a PTDO, followed by the design of a prescribed performance trajectory tracking controller. Section 5 constructs CBFs based on the PTDO and then proposes a safety-critical trajectory tracking control strategy for the UAV within the QP framework. Section 6 provides simulation results to verify the effectiveness of the proposed method. Finally, Section 7 concludes the paper.

Notations: Let $\mathbb{R}$ denote the set of real numbers, and $\mathbb{R}_{\geq 0} = \{a \in \mathbb{R} | a \geq 0\}$. $\mathbb{R}^d$ represents the d-dimensional Euclidean space; $\mathbb{R}^{m\times n}$ denotes the set of $m \times n$ real matrices; $\mathbf{I}_n$ represents the n dimensional identity matrix. For a given vector or matrix $\mathbf{A}$, $\mathbf{A}^{\mathrm{T}}$ denotes its transpose. If matrix $\mathbf{A}$ is invertible, $\mathbf{A}^{-1}$ denotes its inverse. Given two vectors $\mathbf{A} = [a_i]$ and $\mathbf{B} = [b_i]$ of the same dimension, $\mathbf{A}\circ\mathbf{B}$ indicates that $a_i \circ b_i$ for all i with $\circ \in \{>, <, \geq, \leq, =\}$ and $\max(\mathbf{A}, \mathbf{B}) = [\max(a_i, b_i)]$. Define the function $\mathrm{sig}^{\beta}(\cdot) = |\cdot|^{\beta}\mathrm{sign}(\cdot)$, where $\mathrm{sign}(\cdot)$ is the sign function. For a vector argument $\mathbf{x}$, $\mathrm{sig}^{\beta}(\mathbf{x})$ and $\mathrm{sig}(\mathbf{x})$ are defined element-wise. A function $\alpha : \mathbb{R}\to\mathbb{R}$ is said to belong to class $\mathscr{K}_{\infty}^{e}$ ($\alpha \in \mathscr{K}_{\infty}^{e}$), if it is continuous, strictly increasing, satisfies $\alpha(0) = 0$ and $\lim_{x\to\pm\infty}\alpha(x) = \pm\infty$. Examples include $\alpha(x) = ax$ or $\alpha(x) = ax^3$ with $a > 0$. For simplicity, the time index t will be omitted where no ambiguity arises.

2. Problem statement and preliminaries

2.1. Fixed-wing UAV dynamic model

The dynamic model of the fixed-wing UAV is formulated using the following two coordinate frames: (1) the inertial frame $F_I = \{O_I - X_I Y_I Z_I\}$, and (2) the body-fixed frame $F_b = \{o_b - x_b y_b z_b\}$, whose origin coincides with the center of mass of the UAV. Based on these frames, the UAV dynamics can be expressed as follows [49]:

$$\begin{cases} \dot{x} = V\cos\theta\cos\psi + d_x \\ \dot{y} = V\cos\theta\sin\psi + d_y \\ \dot{z} = V\sin\theta + d_z \end{cases} \tag{1}$$

$$\begin{cases} \dot{V} = \dfrac{T-D}{m} - g\sin\theta + d_V \\ \dot{\theta} = \dfrac{L\cos\phi}{mV} - \dfrac{g\cos\theta}{V} + d_\theta \\ \dot{\psi} = \dfrac{L\sin\phi}{mV\cos\theta} + d_\psi \end{cases} \tag{2}$$

where $\mathbf{p} = [x, y, z]^{\mathrm{T}}$ denotes the position of the UAV in the inertial frame F_I; V is the airspeed; θ, ψ and ϕ represent the flight path angle, heading angle, and roll angle, respectively; T, L and D denote the engine thrust, lift, and drag, respectively; m is the mass of the UAV; g is the gravitational acceleration; d_x, d_y, d_z, d_V, d_θ and d_ψ represent unknown external disturbances acting on the state variables, such as natural wind or unmodeled dynamics. The control inputs are selected as the thrust T, the roll angle ϕ, and the lift force L. Specifically, the thrust T is regulated via throttle control, the roll angle ϕ via rudder and aileron actuation, and the lift L via the elevator. For the convenience of simulation, the indirect control input is defined as $\mathbf{u} = [T, L\cos\phi, L\sin\phi]^{\mathrm{T}}$. The fixed-wing UAV model and variable definitions are illustrated in Fig. 1.

Let $\mathbf{v} = \dot{\mathbf{p}} = [v_x, v_y, v_z]^{\mathrm{T}}$ denote the velocity vector of the UAV. Taking the derivative of (1) and substituting (2) into the result yields the following compact form:

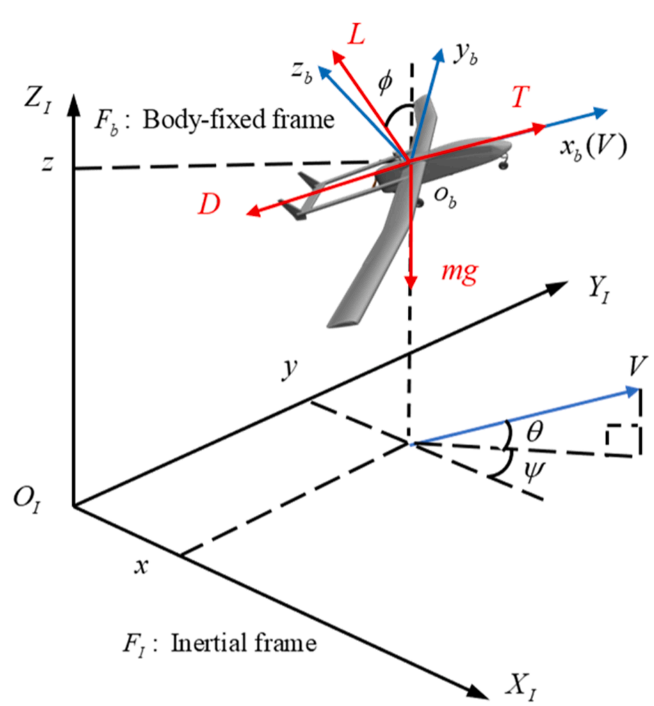

Fig. 1. Fixed-wing UAV model and variable descriptions.

$$\begin{cases} \dot{\mathbf{p}} = \mathbf{v} \\ \dot{\mathbf{v}} = \dfrac{\mathbf{R}}{m}\mathbf{u} + \boldsymbol{\alpha} + \mathbf{d} \end{cases} \tag{3}$$

where

$$\mathbf{R} = \begin{bmatrix} \cos\theta\cos\psi & -\sin\theta\cos\psi & -\sin\psi \\ \cos\theta\sin\psi & -\sin\theta\sin\psi & \cos\psi \\ \sin\theta & \cos\theta & 0 \end{bmatrix}; \boldsymbol{\alpha} = \frac{1}{m}\begin{bmatrix} -D\cos\theta\cos\psi \\ -D\cos\theta\sin\psi \\ -D\sin\theta - mg \end{bmatrix};$$

$\mathbf{d} = \begin{bmatrix} \dot{d}_x + d_V\cos\theta\cos\psi - Vd_\theta\sin\theta\cos\psi - Vd_\psi\cos\theta\sin\psi \\ \dot{d}_y + d_V\cos\theta\sin\psi - Vd_\theta\sin\theta\sin\psi + Vd_\psi\cos\theta\cos\psi \\ \dot{d}_z + d_V\sin\theta + Vd_\theta\cos\theta \end{bmatrix}$ represents the lumped disturbance acting on the UAV.

2.2. Control Barrier Functions

Consider a nonlinear affine system:

$$\dot{\mathbf{x}} = \mathbf{f}(\mathbf{x}) + \mathbf{g}(\mathbf{x})\mathbf{u} \tag{4}$$

where $\mathbf{x} \in \mathbb{R}^n$ and $\mathbf{u} \in \mathbb{R}^m$ denote the system state and control input, respectively. The functions $\mathbf{f}(\mathbf{x}) : \mathbb{R}^n \to \mathbb{R}^n$ and $\mathbf{g}(\mathbf{x}) : \mathbb{R}^n \to \mathbb{R}^{n\times m}$ are assumed to be locally Lipschitz continuous. Furthermore, it is assumed that system (4) is forward complete, i.e., for any initial state $\mathbf{x}(0)$, there exists a unique solution defined on $t \in [0, \infty)$.

The safe set is defined as the 0-superlevel set of a continuously differentiable function $h : \mathbb{R}^n \to \mathbb{R}$, specifically:

$$C = \{\mathbf{x} \in \mathbb{R}^n : h(\mathbf{x}) \geq 0\} \tag{5}$$

The set C is assumed to be nonempty and free of isolated points.

Definition 1. A set C is called a forward invariant set with respect to system (4) if for any initial state $\mathbf{x}(0) \in C$, it holds that $\mathbf{x}(t) \in C$ for all $t \geq 0$. In other words, the safety of (4) is equivalent to the forward invariance of the set C.

Given a safe set C and a function $h(\mathbf{x})$, CBF theory provides a systematic framework for synthesizing controllers with provable safety guarantees. This theory characterizes the influence of the control input $\mathbf{u}$ on system safety by analyzing the derivative of $h(\mathbf{x})$.

Definition 2. For the set C defined by Eq. (5), a continuously differentiable function $h(\mathbf{x})$ is called a CBF for system (4) on C, if there exists $\alpha \in \mathscr{K}_\infty^e$ such that for all $\mathbf{x} \in C$:

$$\sup_{\mathbf{u}\in\mathbb{R}^m} \{L_f h(\mathbf{x}) + L_g h(\mathbf{x})\mathbf{u}\} \geq -\alpha(h(\mathbf{x})) \tag{6}$$

where $L_f h(\mathbf{x}) = \frac{\partial h(\mathbf{x})}{\partial \mathbf{x}}\mathbf{f}(\mathbf{x})$ and $L_g h(\mathbf{x}) = \frac{\partial h(\mathbf{x})}{\partial \mathbf{x}}\mathbf{g}(\mathbf{x})$.

Lemma 1. [32] If $h(\mathbf{x})$ is a CBF on the set C for system (4), then any locally Lipschitz continuous controller $\mathbf{u}$ that satisfies:

$$L_f h(\mathbf{x}) + L_g h(\mathbf{x})\mathbf{u} \geq -\alpha(h(\mathbf{x})) \tag{7}$$

ensures the safety of (4) with respect to C.

Noted that if the relative degree of the control input $\mathbf{u}$ with respect to the function $h(\mathbf{x})$ is greater than 1, the derivative of $h(\mathbf{x})$ does not directly depend on $\mathbf{u}$. In this case, the function $h(\mathbf{x})$ cannot be directly used to construct a safety controller. The high-order CBFs method can be adopted, which constructs a CBF base on $h(\mathbf{x})$. The main idea of high-order CBFs is to introduce $\dot{h}(\mathbf{x}) + \alpha(h(\mathbf{x}))$ as a high-order CBF:

$$h_e(\mathbf{x}) = L_f h(\mathbf{x}) + L_g h(\mathbf{x})\mathbf{u} + \alpha(h(\mathbf{x})) \tag{8}$$

whose 0-superlevel set is $C_e = \{\mathbf{x} \in \mathbb{R}^n : h_e(\mathbf{x}) \geq 0\}$. If the high-order CBF $h_e(\mathbf{x})$ remains nonnegative, system safety can be guaranteed according to Eq. (7), similar to the case in which $h(\mathbf{x})$ serves as a CBF. Further technical details are provided in [33,34].

Therefore, if the controller $\mathbf{u}$ is designed such that Eq. (7) holds for all $\mathbf{x} \in C$, the closed-loop system will remain entirely within the safe set: $\mathbf{x}(0) \in C \Rightarrow \mathbf{x}(t) \in C, \forall t \geq 0$. Eq. (7) is commonly used as a constraint in an optimization problem to synthesize a safety-critical controller. For instance, a nominal controller $\mathbf{u}_d(\mathbf{x}) : \mathbb{R}^n \to \mathbb{R}^m$, which may not guarantee safety, can be modified into a safety-critical controller using QP, as follows:

$$\begin{aligned} &\mathbf{u}_s(\mathbf{x}) = \underset{\mathbf{u}\in\mathbb{R}^m}{argmin} \parallel \mathbf{u} - \mathbf{u}_d(\mathbf{x}) \parallel \\ &\text{s.t. } L_f h(\mathbf{x}) + L_g h(\mathbf{x})\mathbf{u} \geq -\alpha(h(\mathbf{x})) \end{aligned} \tag{9}$$

The optimization problem is formulated to minimize the deviation between the safety control input and the nominal control input.

The controller that satisfies Eq. (7) may no longer be sufficient to guarantee the safe of system in the presence of unknown disturbances. Consider the system:

$$\dot{\mathbf{x}} = \mathbf{f}(\mathbf{x}) + \mathbf{g}(\mathbf{x})\mathbf{u} + \mathbf{d}(\mathbf{x}, \mathbf{p}) \tag{10}$$

where disturbance $\mathbf{p} \in \mathbb{R}^q$ and function $\mathbf{d}(\mathbf{x}, \mathbf{p}) : \mathbb{R}^n \times \mathbb{R}^q \to \mathbb{R}^n$. Note that $\mathbf{p}$ and $\mathbf{d}(\mathbf{x}, \mathbf{p})$ are unknown. Consider the time derivative of $h(\mathbf{x})$ along the system (10):

$$\dot{h}(\mathbf{x}) = L_f h(\mathbf{x}) + L_g h(\mathbf{x})\mathbf{u} + \frac{\partial h(\mathbf{x})}{\partial \mathbf{x}}\mathbf{d}(\mathbf{x}, \mathbf{p}) \tag{11}$$

If $\frac{\partial h(\mathbf{x})}{\partial \mathbf{x}}\mathbf{d}(\mathbf{x}, \mathbf{p})$ is negative on the boundary of the safe set ($h(\mathbf{x}) = 0$), the controller that satisfies Eq. (7) ($L_f h(\mathbf{x}) + L_g h(\mathbf{x})\mathbf{u} \geq 0$) may fail to guarantee that $\dot{h}(\mathbf{x})$ remains nonnegative, implying that the system (10) will leave the safe set.

2.3. Problem Formulation

Let $\mathbf{p}_d(t) = [x_d(t), y_d(t), z_d(t)]^{\mathrm{T}}$ denote the desired trajectory. The trajectory tracking error of the UAV is defined as $\mathbf{e} = \mathbf{p} - \mathbf{p}_d = [e_x, e_y, e_z]^{\mathrm{T}}$. Consider a scenario with M obstacles in the environment, which may be either static or dynamic. Let the position of the j-th obstacle at time t be denoted by $\mathbf{p}_j(t) \in \mathbb{R}^3$, and its geometry characterized by a radius $r_j > 0$. The control objective of this study is to design a safety-critical trajectory tracking controller for a fixed-wing UAV subject to unknown disturbances and prescribed performance requirements, such that the following goals are achieved:

1. Design performance functions $\rho_{i,u}(t)$ and $\rho_{i,l}(t)$ for the tracking error $e_i, i = x, y, z$ to establish a quantitative relationship between control performance (both transient and steady-state) and performance requirements, such as overshoot, steady-state accuracy, and convergence time. These functions should also ensure that the initial error $e_i(0)$ naturally satisfies the constraint, i.e., $\rho_{i,l}(0) < e_i(0) < \rho_{i,u}(0)$.
2. Develop a prescribed performance trajectory tracking controller $\mathbf{u}_d$ to ensure that the tracking error $e_i, i = x, y, z$ remains within the boundaries defined by the performance functions, i.e., $\{e_i | \rho_{i,l}(t) < e_i(t) < \rho_{i,u}(t)\}$.
3. Construct CBFs based on a PTDO, and modify the nominal control input $\mathbf{u}_d$ into a safety-critical control input $\mathbf{u}_s$ via QP, ensuring that the UAV trajectory always satisfies the obstacle avoidance constraints:

$$\parallel \mathbf{p}(t) - \mathbf{p}_j(t) \parallel \geq r_j + r_s, j = 1, \ldots, M$$

where $r_s > 0$ denotes the minimum safe distance required for obstacle avoidance.

4. Design nonnegative adaptive adjustment signals $\lambda_{1,u}^i(t)$ and $\lambda_{1,l}^i(t)$ for the tracking error $e_i, i = x, y, z$ such that: when $\mathbf{u}_s \neq \mathbf{u}_d$, the performance boundaries are relaxed, i.e., $\left\{e_i \middle| \rho_{i,l}(t) - \lambda_{1,l}^i(t) < e_i(t) < \rho_{i,u}(t) + \lambda_{1,u}^i(t)\right\}$, and when $\mathbf{u}_s = \mathbf{u}_d$, the signals $\lambda_{1,u}^i(t)$ and $\lambda_{1,l}^i(t)$ exponentially decay to zero, thereby recovering the original performance constraints.

The following assumption is made in this paper.

Assumption 1. The desired trajectory $\mathbf{p}_d(t)$ is twice continuously differentiable and bounded.

Remark 1. Assumption 1 is widely adopted in trajectory tracking control strategies for various practical systems [9,22,35], and is naturally satisfied by many trajectory planners, such as B-splines and minimum-snap, which typically generate trajectories with second-order or higher continuity.

Fig. 2 illustrates the overall framework of the proposed control scheme.

2.4. Mathematical Lemmas

Lemma 2. [50] For a Metzler matrix $\mathbf{W} \in \mathbb{R}^{m\times m}$ (i.e., a matrix with nonnegative off-diagonal elements) and a vector $\mathbf{q}(t) \in \mathbb{R}^m_{\geq 0}, \forall t \geq 0$, the system $\dot{\mathbf{p}}(t) = \mathbf{W}\mathbf{p}(t) + \mathbf{q}(t)$ admits a unique solution $\mathbf{p}(t)$ for any initial condition $\mathbf{p}(0) \in \mathbb{R}^m$. Moreover, if $\mathbf{p}(0) \in \mathbb{R}^m_{\geq 0}$, then the solution satisfies $\mathbf{p}(t) \geq \boldsymbol{0}$ for all $t \geq 0$.

Lemma 3. [51] Consider a nonlinear system $\dot{\mathbf{x}} = \mathbf{f}(\mathbf{x}(t))$. If there exists a radially unbounded Lyapunov function $V(\mathbf{x})$ such that:

$$\dot{V}(\mathbf{x}) \leq -\frac{\pi}{\gamma T_c}\left(V^{1-\frac{\gamma}{2}}(\mathbf{x}) + V^{1+\frac{\gamma}{2}}(\mathbf{x})\right)$$

where $T_c > 0$ and $0 < \gamma < 1$, then the equilibrium of the system is predefined-time stable with the predefined-time T_c.

Lemma 4. [52] For $x_i \geq 0, i = 1, \ldots, n$ and $\gamma > 0$, the following inequalities hold:

$$\begin{cases} \sum_{i=1}^{n} x_i^\gamma \geq \left(\sum_{i=1}^{n} x_i\right)^\gamma, \text{if } 0 < \gamma < 1 \\ \sum_{i=1}^{n} x_i^\gamma \geq n^{1-\gamma}\left(\sum_{i=1}^{n} x_i\right)^\gamma, \text{if } \gamma > 1 \end{cases}$$

3. Design of Performance Functions and Adaptive Adjustment Signals

In order to satisfy the prescribed performance requirements, such as overshoot, steady-state accuracy, and convergence time, while ensuring system flexibility under safety constraints, this section presents the design of polynomial performance functions together with adaptive adjustment signals.

3.1. Polynomial performance functions

For the tracking error $e_i(t), i = x, y, z$, the following PPFs $\rho_{i,u}(t)$ and $\rho_{i,l}(t)$ are defined to specify its upper and lower boundaries, respectively:

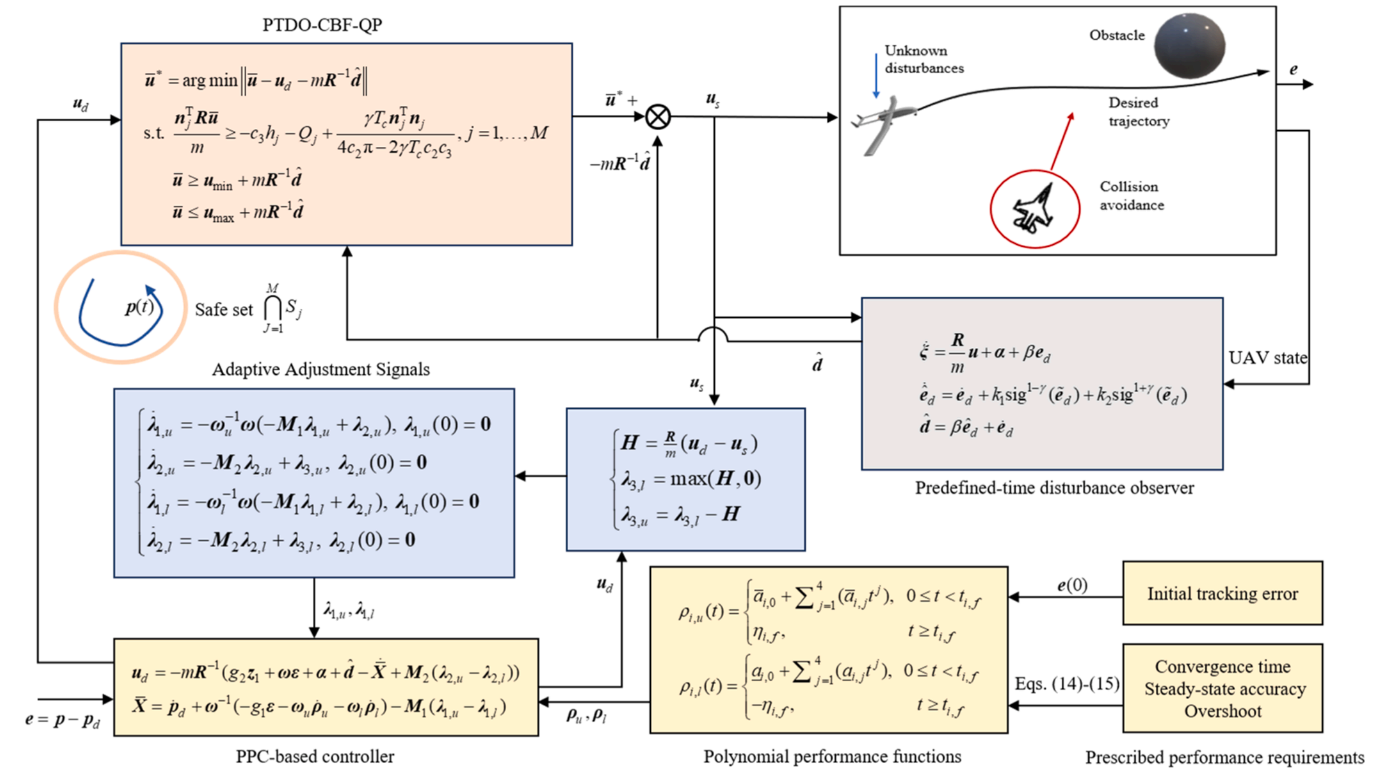

Fig. 2. Overall framework of the proposed control scheme. The potentially unsafe PPC-based controller is enhanced with a PTDO and CBFs to ensure that the UAV maintains a safe distance from obstacles at all times.

$$\rho_{i,u}(t) = \begin{cases} \bar{a}_{i,0} + \sum_{j=1}^{4} \left(\bar{a}_{i,j} t^j\right), 0 \le t < t_{i,f} \\ \eta_{i,f}, t \ge t_{i,f} \end{cases} \tag{12}$$

$$\rho_{i,l}(t) = \begin{cases} \underline{a}_{i,0} + \sum_{j=1}^{4} \left(\underline{a}_{i,j} t^j\right), 0 \le t < t_{i,f} \\ -\eta_{i,f}, t \ge t_{i,f} \end{cases} \tag{13}$$

where $t_{i,f}$ denotes the desired convergence time, and $\eta_{i,f} > 0$ represents the maximum allowable steady-state magnitude of $e_i(t)$. The design parameters $\bar{a}_{i,j}$ and $\underline{a}_{i,j}, j \in \{0, 1, 2, 3, 4\}$ can be determined by solving the following equations:

$$\begin{cases} \rho_{i,u}(0) = \bar{a}_{i,0} = e_i(0) + \bar{\eta}_{i,0} \\ \dot{\rho}_{i,u}(0) = \bar{a}_{i,1} = 0 \\ \rho_{i,u}\left(t_{i,f}\right) = \bar{a}_{i,0} + \sum_{j=1}^{4} \left(\bar{a}_{i,j} t_{i,f}^j\right) = \eta_{i,f} \\ \dot{\rho}_{i,u}\left(t_{i,f}\right) = \bar{a}_{i,1} + 2\bar{a}_{i,2} t_{i,f} + 3\bar{a}_{i,3} t_{i,f}^2 + 4\bar{a}_{i,4} t_{i,f}^3 = 0 \\ \ddot{\rho}_{i,u}\left(t_{i,f}\right) = 2\bar{a}_{i,2} + 6\bar{a}_{i,3} t_{i,f} + 12\bar{a}_{i,4} t_{i,f}^2 = 0 \end{cases} \tag{14}$$

$$\begin{cases} \rho_{i,l}(0) = \underline{a}_{i,0} = e_i(0) - \underline{\eta}_{i,0} \\ \dot{\rho}_{i,l}(0) = \underline{a}_{i,1} = 0 \\ \rho_{i,l}\left(t_{i,f}\right) = \underline{a}_{i,0} + \sum_{j=1}^{4} \left(\underline{a}_{i,j} t_{i,f}^j\right) = -\eta_{i,f} \\ \dot{\rho}_{i,l}\left(t_{i,f}\right) = \underline{a}_{i,1} + 2\underline{a}_{i,2} t_{i,f} + 3\underline{a}_{i,3} t_{i,f}^2 + 4\underline{a}_{i,4} t_{i,f}^3 = 0 \\ \ddot{\rho}_{i,l}\left(t_{i,f}\right) = 2\underline{a}_{i,2} + 6\underline{a}_{i,3} t_{i,f} + 12\underline{a}_{i,4} t_{i,f}^2 = 0 \end{cases} \tag{15}$$

where $\bar{\eta}_{i,0} > 0$ and $\underline{\eta}_{i,0} > 0$ are parameters associated with the overshoot.

Therefore, by appropriately designing the PPFs $\rho_{i,u}(t)$ and $\rho_{i,l}(t)$, $i = x, y, z$, a quantitative relationship can be established between control performance and performance requirements. Moreover, the influence of the initial tracking error $e_i(0)$ is explicitly considered in the design of the performance functions, which ensures that the initial condition $\rho_{i,l}(0) < e_i(0) < \rho_{i,u}(0)$ is naturally satisfied.

Remark 2. The coefficients of the PPFs can be explicitly related to the prescribed performance requirements. Once these requirements are determined, the corresponding performance functions can be systematically designed. The proposed PPFs are intuitively shown in Fig. 3, from which it is evident that both the convergence time and the steady-state tracking error can be quantitatively specified. Additionally, the overshoot of $e(t)$ is approximately zero. Note that at $t = 0$, $\dot{\rho}_{i,u}(0) = 0$ and $\dot{\rho}_{i,l}(0) = 0$, which ensures the smoothness of the controller output during the initial phase. Furthermore, the performance functions $\rho_{i,u}(t)$ and $\rho_{i,l}(t)$ are twice continuously differentiable over time, which is sufficient to support the subsequent controller design. However, in applications that require higher-order continuity (e.g., $C^n, n > 2$), a higher-order polynomial performance function can be adopted as follows:

$$\rho(t) = \begin{cases} a_0 + \sum_{j=1}^{n+2} \left(a_j t^j\right), 0 \le t < t_f \\ \eta_f, t \ge t_f \end{cases}$$

where the coefficients $a_j, j = 0, 1, \ldots, n+2$ are determined by algebraic conditions similar to those in Eqs. (14) and (15).

3.2. Adaptive Adjustment Signals

To avoid the singularity problem of PPC arising from enforcing obstacle avoidance safety, the nonnegative adaptive adjustment signals $\lambda_{1,u}^i(t)$ and $\lambda_{1,l}^i(t)$ are introduced for the tracking error $e_i(t), i = x, y, z$, aiming to dynamically modify the performance boundaries. The

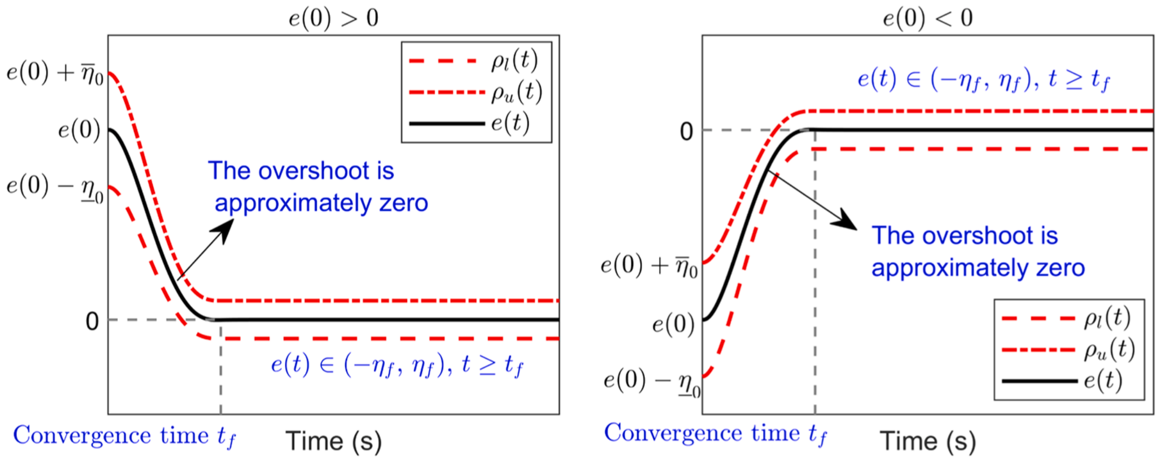

Fig. 3. Illustration of the proposed polynomial performance functions.

adjusted performance boundaries are defined as $E_{i,u}(t) = \rho_{i,u}(t) + \lambda_{1,u}^i(t)$ and $E_{i,l} = \rho_{i,l}(t) - \lambda_{1,l}^i(t)$. The tracking error $e_i(t)$ is required to evolve strictly within these boundaries:

$$E_{i,l}(t) < e_i(t) < E_{i,u}(t) \tag{16}$$

To facilitate the controller design process, the constrained system (16) is transformed into an equivalent unconstrained form. To this end, a transformed error $\varepsilon_i(t)$ is defined as follows:

$$\varepsilon_i(t) = \text{In}\left(\frac{e_i(t) - E_{i,l}(t)}{E_{i,u}(t) - e_i(t)}\right) \tag{17}$$

Let $\boldsymbol{\rho}_u, \boldsymbol{\rho}_l, \boldsymbol{\lambda}_{1,u}, \boldsymbol{\lambda}_{1,l}, \mathbf{E}_u, \mathbf{E}_l, \boldsymbol{\varepsilon}$ be the stack vector of $\rho_{i,u}, \rho_{i,l}, \lambda_{1,u}^i, \lambda_{1,l}^i, E_{i,u}, E_{i,l}, \varepsilon_i$, respectively. Under the constraint (16) and the transformation (17), the following diagonal matrices are defined: $\boldsymbol{\omega} = \partial\boldsymbol{\varepsilon}/\partial\mathbf{e}$, $\boldsymbol{\omega}_u = \partial\boldsymbol{\varepsilon}/\partial\mathbf{E}_u$, $\boldsymbol{\omega}_l = \partial\boldsymbol{\varepsilon}/\partial\mathbf{E}_l$, all of which are invertible. The adaptive adjustment signals $\boldsymbol{\lambda}_{1,u}$ and $\boldsymbol{\lambda}_{1,l}$ are generated by the following auxiliary system:

$$\begin{cases} \dot{\boldsymbol{\lambda}}_{1,u} = -\boldsymbol{\omega}_u^{-1}\boldsymbol{\omega}\left(-\mathbf{M}_1\boldsymbol{\lambda}_{1,u} + \boldsymbol{\lambda}_{2,u}\right), \boldsymbol{\lambda}_{1,u}(0) = \boldsymbol{0} \\ \dot{\boldsymbol{\lambda}}_{2,u} = -\mathbf{M}_2\boldsymbol{\lambda}_{2,u} + \boldsymbol{\lambda}_{3,u}, \boldsymbol{\lambda}_{2,u}(0) = \boldsymbol{0} \\ \dot{\boldsymbol{\lambda}}_{1,l} = -\boldsymbol{\omega}_l^{-1}\boldsymbol{\omega}\left(-\mathbf{M}_1\boldsymbol{\lambda}_{1,l} + \boldsymbol{\lambda}_{2,l}\right), \boldsymbol{\lambda}_{1,l}(0) = \boldsymbol{0} \\ \dot{\boldsymbol{\lambda}}_{2,l} = -\mathbf{M}_2\boldsymbol{\lambda}_{2,l} + \boldsymbol{\lambda}_{3,l}, \boldsymbol{\lambda}_{2,l}(0) = \boldsymbol{0} \end{cases} \tag{18}$$

where $\boldsymbol{\lambda}_{3,l} = \max(\mathbf{H}, \boldsymbol{0})$, $\boldsymbol{\lambda}_{3,u} = \boldsymbol{\lambda}_{3,l} - \mathbf{H}$ with $\mathbf{H} = \frac{\mathbf{R}}{m}(\mathbf{u}_d - \mathbf{u}_s)$; M_1 and M_2 are diagonal positive definite matrices.

The adaptive adjustment signals $\boldsymbol{\lambda}_{1,u}$ and $\boldsymbol{\lambda}_{1,l}$ are directly related to the input error $(\mathbf{u}_d - \mathbf{u}_s)$, which is defined as the difference between the safe control input $\mathbf{u}_s$ and the nominal control input $\mathbf{u}_d$. These signals are incorporated into the performance functions $\boldsymbol{\rho}_u$ and $\boldsymbol{\rho}_l$ to guarantee the reliable operation of PPC, even under strict safety requirements. The proposed auxiliary system possesses the following property.

Theorem 1. Consider the fixed-wing UAV (3), the auxiliary system (18), and the transformed error defined in (17). Suppose there exists a constant vector $\overline{\mathbf{b}} \in \mathbb{R}^3_{\geq 0}$, such that the inequality $|\mathbf{H}| \leq \overline{\mathbf{b}}$ holds, and the tracking error $\mathbf{e}$ satisfies the condition $\mathbf{E}_l(t) < \mathbf{e}(t) < \mathbf{E}_u(t)$, then $\boldsymbol{0} \leq \boldsymbol{\lambda}_{j,u}$, $\boldsymbol{\lambda}_{j,l} \leq \prod_j^2 \left(\mathrm{M}_j^{-1}\right)\overline{\mathbf{b}}, j = 1, 2$.

Proof. Since $\boldsymbol{\lambda}_{2,u}(0)$, $\boldsymbol{\lambda}_{2,l}(0)$, $\boldsymbol{\lambda}_{3,u}(t)$ and $\boldsymbol{\lambda}_{3,l}(t)$ are all nonnegative, and the matrix $-\mathrm{M}_2$ is a diagonal (Metzler) matrix, it follows from Lemma 2 that $\boldsymbol{\lambda}_{2,u}, \boldsymbol{\lambda}_{2,l} \geq \boldsymbol{0}$.With the inequality $|\mathbf{H}| \leq \overline{\mathbf{b}}$, it can obtain that $\boldsymbol{\lambda}_{3,u} \leq \overline{\mathbf{b}} = \left[\overline{b}_x, \overline{b}_y, \overline{b}_z\right]^{\mathrm{T}}$. Let $\boldsymbol{\lambda}_{2,u} = \left[\lambda_{2,u}^x, \lambda_{2,u}^y, \lambda_{2,u}^z\right]$, then for each $i = x, y, z$, the dynamics of $\lambda_{2,u}^i$ satisfies $\dot{\lambda}_{2,u}^i \leq -\mathrm{M}_{2,i}\lambda_{2,u}^i + \overline{b}_i$, where $\mathrm{M}_{2,i}$ is diagonal element of M_2. Therefore, when $\dot{\lambda}_{2,u}^i < 0$, one has $\lambda_{2,u}^i > \overline{b}_i/\mathrm{M}_{2,i}$, which implies $\boldsymbol{0} \leq \boldsymbol{\lambda}_{2,u} \leq \mathrm{M}_2^{-1}\overline{\mathbf{b}}$. Similarly, one can obtain $\boldsymbol{0} \leq \boldsymbol{\lambda}_{2,u} \leq \mathrm{M}_2^{-1}\overline{\mathbf{b}}$.

When the tracking error $\mathbf{e}$ satisfies $\mathbf{E}_l(t) < \mathbf{e}(t) < \mathbf{E}_u(t)$, both $-\boldsymbol{\omega}_u^{-1}\boldsymbol{\omega}$ and $-\boldsymbol{\omega}_l^{-1}\boldsymbol{\omega}$ are diagonal positive definite matrices. Since $\boldsymbol{\lambda}_{1,u}(0)$, $\boldsymbol{\lambda}_{1,l}(0)$, $\boldsymbol{\lambda}_{2,u}(t)$ and $\boldsymbol{\lambda}_{2,l}(t)$ remain nonnegative, and the matrix $-\mathrm{M}_1$ is diagonal (Metzler), Lemma 2 again implies that $\boldsymbol{\lambda}_{1,u}, \boldsymbol{\lambda}_{1,l} \geq \boldsymbol{0}$. For each $\boldsymbol{i} = x, y, z$, the dynamics of $\lambda_{1,u}^i$follows $\dot{\lambda}_{1,u}^i \leq -\frac{\omega_i}{\omega_{u,i}}\left(-\mathrm{M}_{1,i}\lambda_{1,u}^i + \overline{b}_i/\mathrm{M}_{2,i}\right)$, where $\omega_i > 0$, $\omega_{u,i} < 0$ and $\mathrm{M}_{1,i}$ are diagonal elements of $\boldsymbol{\omega}$, $\boldsymbol{\omega}_u$ and M_1, respectively. Thus, when $\lambda_{1,u}^i > \overline{b}_i/\left(\mathrm{M}_{1,i}\mathrm{M}_{2,i}\right)$, it can be concluded that $\dot{\lambda}_{1,u}^i < 0$, implying $\boldsymbol{0} \leq \boldsymbol{\lambda}_{1,u} \leq \mathrm{M}_1^{-1}\mathrm{M}_2^{-1}\overline{\mathbf{b}}$. Likewise, one can derive that $\boldsymbol{0} \leq \boldsymbol{\lambda}_{1,l} \leq \mathrm{M}_1^{-1}\mathrm{M}_2^{-1}\overline{\mathbf{b}}$. This completes the proof of Theorem 1.

Remark 3. According to Theorem 1, by leveraging positive system theory (Lemma 2), it is guaranteed that the states of the auxiliary system remain nonnegative. Consequently, the adaptive adjustment signals $\boldsymbol{\lambda}_{1,u}$ and $\boldsymbol{\lambda}_{1,l}$ serve solely to relax the performance boundaries. Specifically, the auxiliary system establishes a feedback mechanism from the safety constraints to the performance constraints. The signals $\boldsymbol{\lambda}_{3,u}$ and $\boldsymbol{\lambda}_{3,l}$ are dynamically updated based on the input error $(\mathbf{u}_d - \mathbf{u}_s)$, which determine the unreachable increasing and decreasing rates for the UAV state $\mathbf{v}$. From (18), adaptive adjustment signals $\boldsymbol{\lambda}_{1,u}$ and $\boldsymbol{\lambda}_{1,l}$ are obtained by gradual integration, thereby quantifying the performance degradation induced by the need to satisfy safety constraints. When the UAV performs obstacle avoidance, these nonnegative signals adjust dynamically, resulting in a temporary relaxation of the performance boundaries. In contrast, when obstacle avoidance is not required, $\boldsymbol{\lambda}_{3,u} = \boldsymbol{0}$ and $\boldsymbol{\lambda}_{3,l} = \boldsymbol{0}$, along with the damping terms $-\mathrm{M}_j\boldsymbol{\lambda}_{j,u}$ and $-\mathrm{M}_j\boldsymbol{\lambda}_{j,l}, j = 1, 2$, ensure that $\boldsymbol{\lambda}_{1,u}$ and $\boldsymbol{\lambda}_{1,l}$ converge to zero exponentially. This implies that the relaxed

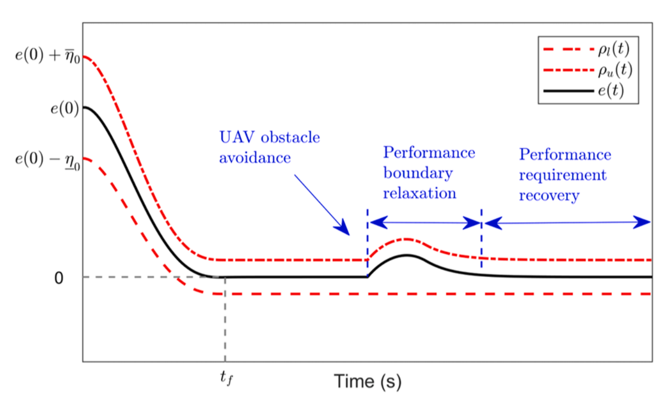

Fig. 4. The adjustment process of the performance boundary.

boundaries recover to the prescribed performance requirements. Fig. 4 illustrates the adjustment process of the performance boundary.

4. Prescribed performance trajectory tracking control

In this section, a PTDO is designed to accurately estimate the lumped disturbances in the UAV flight. Then, a prescribed performance trajectory tracking controller is developed to ensure that the tracking errors remain strictly within the performance boundaries.

4.1. Predefined-time disturbance observer

Inspired by the design concept of the fixed-time disturbance observer in [52], an auxiliary variable is defined as

$$\dot{\xi} = \frac{\mathbf{R}}{m}\mathbf{u} + \boldsymbol{\alpha} + \beta\mathbf{e}_d \tag{19}$$

where $\mathbf{e}_d = \mathbf{v} - \boldsymbol{\xi}$, and $\beta > 0$ is a constant. Then, the PTDO is developed as follows:

$$\widehat{\mathbf{d}} = \beta\widehat{\mathbf{e}}_d + \dot{\mathbf{e}}_d \tag{20}$$

where $\widehat{\mathbf{d}} = \left[\widehat{d}_x, \widehat{d}_y, \widehat{d}_z\right]^{\mathrm{T}}$ denotes the estimation of the lumped disturbance $\mathbf{d}$, and $\widehat{\mathbf{e}}_d$ is the state estimation of $\mathbf{e}_d$, which is given by

$$\dot{\widehat{\mathbf{e}}}_d = \dot{\mathbf{e}}_d + k_1\mathrm{sig}^{1-\gamma}(\widetilde{\mathbf{e}}_d) + k_2\mathrm{sig}^{1+\gamma}(\widetilde{\mathbf{e}}_d) \tag{21}$$

where $\widetilde{\mathbf{e}}_d = \mathbf{e}_d - \widehat{\mathbf{e}}_d$ is the state estimation error, $0 < \gamma < 1$, $k_1 = \frac{\pi}{\gamma T_c}\left(\frac{1}{2}\right)^{1-\frac{\gamma}{2}}$, $k_2 = \frac{\pi}{\gamma T_c}3^{\frac{\gamma}{2}\left(\frac{1}{2}\right)^{1+\frac{\gamma}{2}}}$ and $T_c > 0$ is a predefined convergence time.

Lemma 5. For the fixed-wing UAV (3), under the PTDO (19)-(21), the disturbance estimation error $\widetilde{\mathbf{d}} = \mathbf{d} - \widehat{\mathbf{d}}$ converges to zero within the predefined time T_c.

Proof. According to Eq. (21), the dynamics of the state estimation error $\widetilde{\mathbf{e}}_d$ can be written as:

$$\dot{\widetilde{\mathbf{e}}}_d = -k_1\mathrm{sig}^{1-\gamma}(\widetilde{\mathbf{e}}_d) - k_2\mathrm{sig}^{1+\gamma}(\widetilde{\mathbf{e}}_d) \tag{22}$$

To analyze the convergence of $\widetilde{\mathbf{e}}_d$, consider the Lyapunov function $V_e(\widetilde{\mathbf{e}}_d) = \frac{1}{2}\widetilde{\mathbf{e}}_d^{\mathrm{T}}\widetilde{\mathbf{e}}_d$. From Lemma 4, its time derivative is given by

$$\begin{aligned}
&\dot{V}_e(\widetilde{\mathbf{e}}_d) = -k_1\widetilde{\mathbf{e}}_d^{\mathrm{T}}\mathrm{sig}^{1-\gamma}(\widetilde{\mathbf{e}}_d) - k_2\widetilde{\mathbf{e}}_d^{\mathrm{T}}\mathrm{sig}^{1+\gamma}(\widetilde{\mathbf{e}}_d)\\
&\leq -k_1\sum\nolimits_{j=1}^{3}\left|\widetilde{e}_{dj}\right|^{2-\gamma} - k_2\sum\nolimits_{j=1}^{3}\left|\widetilde{e}_{dj}\right|^{2+\gamma}\\
&\leq -k_1 2^{1-\frac{\gamma}{2}}V_e^{1-\frac{\gamma}{2}} - k_2 3^{-\frac{\gamma}{2}}2^{1+\frac{\gamma}{2}}V_e^{1+\frac{\gamma}{2}}\\
&\leq -\frac{\pi}{\gamma T_c}\left(V_e^{1-\frac{\gamma}{2}} + V_e^{1+\frac{\gamma}{2}}\right)
\end{aligned} \tag{23}$$

From Lemma 3 and Eq. (23), it follows that $\widetilde{\mathbf{e}}_d(t) = \boldsymbol{0}$ for all $t \geq T_c$. Furthermore, by combining Eqs. (3), (19), and (20), the disturbance estimation error $\widetilde{\mathbf{d}}$ can be expressed as:

$$\widetilde{\mathbf{d}} = \mathbf{d} - \beta\widehat{\mathbf{e}}_d - \dot{\mathbf{v}} + \dot{\xi} = \beta\widetilde{\mathbf{e}}_d \tag{24}$$

Therefore, it can be concluded that $\widetilde{\mathbf{d}}(t) = \boldsymbol{0}$ for $t \geq T_c$. This completes the proof of Lemma 5.

4.2. Design of a Prescribed Performance Controller

The boundedness of the transformed error $\boldsymbol{\varepsilon}(t)$ is equivalent to the tracking error $\mathbf{e}(t)$ satisfying the prescribed performance constraint (16). Therefore, the control objective is reformulated as the design of a controller that guarantees the boundedness of $\boldsymbol{\varepsilon}(t)$.

Step1. The derivative of $\boldsymbol{\varepsilon}(t)$ is calculated as

$$\begin{aligned}
&\dot{\varepsilon} = \boldsymbol{\omega}\dot{e} + \boldsymbol{\omega}_u\dot{\mathbf{E}}_u + \boldsymbol{\omega}_l\dot{\mathbf{E}}_l\\
&= \boldsymbol{\omega}(\dot{\mathbf{p}} - \dot{\mathbf{p}}_d) + \boldsymbol{\omega}_u(\dot{\rho}_u + \dot{\lambda}_{1,u}) + \boldsymbol{\omega}_l(\dot{\rho}_l - \dot{\lambda}_{1,l})
\end{aligned} \tag{25}$$

Substituting Eq. (18) into Eq. (25) yields:

$$\begin{aligned}
&\dot{\varepsilon} = \boldsymbol{\omega}(\mathbf{v} - \dot{\mathbf{p}}_d + \lambda_{2,l} - \lambda_{2,u}) + \boldsymbol{\omega}_u\dot{\rho}_u\\
&+\boldsymbol{\omega}_l\dot{\rho}_l + \boldsymbol{\omega}\mathrm{M}_1(\lambda_{1,u} - \lambda_{1,l})
\end{aligned} \tag{26}$$

Define the first Lyapunov function as $V_1(\boldsymbol{\varepsilon}) = \frac{1}{2}\boldsymbol{\varepsilon}^{\mathrm{T}}\boldsymbol{\varepsilon}$, and take its derivative:

$$\begin{aligned}
&\dot{V}_1 = \boldsymbol{\varepsilon}^{\mathrm{T}}\boldsymbol{\omega}(\mathbf{v} - \dot{\mathbf{p}}_d + \lambda_{2,l} - \lambda_{2,u})\\
&+\boldsymbol{\varepsilon}^{\mathrm{T}}(\boldsymbol{\omega}_u\dot{\rho}_u + \boldsymbol{\omega}_l\dot{\rho}_l) + \boldsymbol{\varepsilon}^{\mathrm{T}}\boldsymbol{\omega}\mathrm{M}_1(\lambda_{1,u} - \lambda_{1,l})
\end{aligned} \tag{27}$$

Let $\mathbf{z}_1(t) = \mathbf{v}(t) - \mathbf{v}_d(t)$ be the intermediate error, where $\mathbf{v}_d$ is a virtual velocity command defined by:

$$\mathbf{v}_d = \lambda_{2,u} - \lambda_{2,l} + \overline{\mathbf{X}} \tag{28}$$

where $\overline{\mathbf{X}} = \dot{\mathbf{p}}_d + \boldsymbol{\omega}^{-1}(-g_1\boldsymbol{\varepsilon} - \boldsymbol{\omega}_u\dot{\rho}_u - \boldsymbol{\omega}_l\dot{\rho}_l) - \mathrm{M}_1(\lambda_{1,u} - \lambda_{1,l})$, and $g_1 > 0$ is a control gain. Substituting Eq. (28) into Eq. (27) gives:

$$\dot{V}_1 = \boldsymbol{\varepsilon}^{\mathrm{T}}\boldsymbol{\omega}\mathbf{z}_1 - g_1\boldsymbol{\varepsilon}^{\mathrm{T}}\boldsymbol{\varepsilon} \tag{29}$$

Step 2. Compute the time derivative of $\mathbf{z}_1(t)$:

$$\begin{aligned}
&\dot{\mathbf{z}}_1 = \frac{\mathbf{R}}{m}\mathbf{u}_s + \boldsymbol{\alpha} + \mathbf{d} - \dot{\lambda}_{2,u} + \dot{\lambda}_{2,l} - \dot{\overline{\mathbf{X}}}\\
&= \frac{\mathbf{R}}{m}\mathbf{u}_s + \boldsymbol{\alpha} + \mathbf{d} + \mathrm{M}_2(\lambda_{2,u} - \lambda_{2,l}) + \lambda_{3,l} - \lambda_{3,u} - \dot{\overline{\mathbf{X}}}
\end{aligned} \tag{30}$$

By applying $\lambda_{3,l} - \lambda_{3,u} = \frac{\mathbf{R}}{m}(\mathbf{u}_d - \mathbf{u}_s)$, the dynamics of $\mathbf{z}_1$ in Eq. (30) can be expressed as:

$$\dot{\mathbf{z}}_1 = \frac{\mathbf{R}}{m}\mathbf{u}_d + \boldsymbol{\alpha} + \mathbf{d} + \mathrm{M}_2(\lambda_{2,u} - \lambda_{2,l}) - \dot{\overline{\mathbf{X}}} \tag{31}$$

Define the second Lyapunov function as $V_2 = \frac{1}{2}\mathbf{z}_1^{\mathrm{T}}\mathbf{z}_1 + V_1$, and compute its derivative:

$$\dot{V}_2 = \mathbf{z}_1^{\mathrm{T}}\left(\frac{\mathbf{R}}{m}\mathbf{u}_d + \boldsymbol{\alpha} + \mathbf{d} - \dot{\overline{\mathbf{X}}}\right) + \mathbf{z}_1^{\mathrm{T}}\mathrm{M}_2(\lambda_{2,u} - \lambda_{2,l}) + \dot{V}_1 \tag{32}$$

The prescribed performance controller $\mathbf{u}_d$ is designed as:

$$\mathbf{u}_d = -m\mathbf{R}^{-1}\left(g_2\mathbf{z}_1 + \boldsymbol{\omega}\varepsilon + \boldsymbol{\alpha} + \widehat{\mathbf{d}} - \dot{\overline{\mathbf{X}}} + \mathrm{M}_2(\lambda_{2,u} - \lambda_{2,l})\right) \tag{33}$$

where $g_2 > \frac{1}{2}$ is a control gain. Substituting Eq. (33) into Eq. (32) yields:

$$\dot{V}_2 = \dot{V}_1 - g_2\mathbf{z}_1^{\mathrm{T}}\mathbf{z}_1 - \mathbf{z}_1^{\mathrm{T}}\boldsymbol{\omega}\varepsilon + \mathbf{z}_1^{\mathrm{T}}\widetilde{\mathbf{d}} \tag{34}$$

Theorem 2. For the fixed-wing UAV (3), under Assumptions 1, if the PPFs (12) and (13), the auxiliary system (18), the PTDO (19)-(21), and the prescribed performance controller (33) are adopted, then the closed-loop system is uniformly bounded, and the performance constraint in Eq. (16) is satisfied.

Proof: Substituting Eq. (29) into Eq. (34) gives:

$$\begin{aligned}
&\dot{V}_2 = -g_1\boldsymbol{\varepsilon}^{\mathrm{T}}\boldsymbol{\varepsilon} - g_2\mathbf{z}_1^{\mathrm{T}}\mathbf{z}_1 + \mathbf{z}_1^{\mathrm{T}}\widetilde{\mathbf{d}}\\
&\leq -g_1\boldsymbol{\varepsilon}^{\mathrm{T}}\boldsymbol{\varepsilon} - \left(g_2 - \frac{1}{2}\right)\mathbf{z}_1^{\mathrm{T}}\mathbf{z}_1 + \frac{1}{2}\widetilde{\mathbf{d}}^{\mathrm{T}}\widetilde{\mathbf{d}}\\
&\leq -\vartheta V_2 + \varpi
\end{aligned} \tag{35}$$

where $\vartheta = \min\left\{g_1, g_2 - \frac{1}{2}\right\}$, and $\varpi = \frac{1}{2}\widetilde{\mathbf{d}}^{\mathrm{T}}\widetilde{\mathbf{d}}$. According to Lemma 5, ϖ is bounded. Let $\Delta = \{V_2 | V_2 \le \varpi/\vartheta\}$ be a compact set. It can be concluded that if $V_2 \notin \Delta$, then $\dot{V}_2 < 0$ holds. Therefore, V_2 is bounded and ultimately converges to the set Δ, which implies that the closed-loop system is uniformly bounded. Furthermore, since the transformed error $\boldsymbol{\varepsilon}(t)$ is bounded, the performance constraint in Eq. (16) is satisfied. This completes the proof of Theorem 2.

Remark 4. Consider the scenario without obstacle avoidance, i.e., $\mathbf{u}_s = \mathbf{u}_d$, then $\lambda_{3,u}(t) = \mathbf{0}$ and $\lambda_{3,l}(t) = \mathbf{0}$ for all $t \ge 0$. According to Eq. (18), it can be derived that $\lambda_{1,u}(t) = \mathbf{0}$ and $\lambda_{1,l}(t) = \mathbf{0}$. Therefore, the performance boundaries $\mathbf{E}_u(t)$ and $\mathbf{E}_l(t)$ recover to the corresponding PPFs $\boldsymbol{\rho}_u(t)$ and $\boldsymbol{\rho}_l(t)$, respectively. This implies that, in the absence of obstacle avoidance constraints, the prescribed performance requirements fully determine the constraint in Eq. (16). Consequently, controller (33) also ensures that the tracking error satisfies the PPFs, that is: $\{\mathbf{e}(t) | \boldsymbol{\rho}_l(t) < \mathbf{e}(t) < \boldsymbol{\rho}_u(t)\}$.

5. Safety-Critical Trajectory Tracking Control

This section proposes a robust CBF design method based on the PTDO to ensure obstacle avoidance for UAVs. Furthermore, by embedding the CBF constraints into a QP framework, the PPC-based controller is modified in real time, which results in a safety-critical trajectory tracking controller.

5.1. PTDO-based safety with CBFs

For the UAV $\mathbf{p}(t)$ and obstacle $\mathbf{p}_j(t), j = 1, \ldots, M$, define the following function:

$$\rho_j(t) = \| \boldsymbol{\delta}_j(t) \| - (r_j + r_s) \tag{36}$$

where $\boldsymbol{\delta}_j(t) = \mathbf{p}(t) - \mathbf{p}_j(t)$ denotes the relative position vector between the UAV and the obstacle. The corresponding safe set can be defined as $S_j = \{\mathbf{p} \in \mathbb{R}^3 : \rho_j \ge 0\}$. According to Definition 1, if the set $\cap_{j=1}^{M} S_j$ is forward invariant with respect to the UAV system (3), then collision avoidance is guaranteed.

Since the control input of UAV (3) has a relative degree of 2 with respect to the function ρ_j, a high-order CBF is employed. By defining $h_j = \dot{\rho}_j + c_1 \rho_j$ with $c_1 > 0$, the 0-superlevel set $C_j = \{\mathbf{p} \in \mathbb{R}^3 : h_j \ge 0\}$ is constructed. In this formulation, the relative degree of h_j is 1, which makes the design of CBF-based constraints feasible. However, due to the presence of unknown disturbances in Eq. (3), the strong model dependence of CBF prevents the direct use of the constraint $\dot{h}_j(\mathbf{x}) \ge -\alpha(h_j(\mathbf{x}))$ for constructing a valid safety controller.

To mitigate the impact of unknown disturbances, a CBF design method based on the PTDO is proposed. Lemma 5 indicates that the disturbance estimation error $\tilde{\mathbf{d}}$ is bounded, as characterized by the Lyapunov function $V_d = \frac{1}{2}\tilde{\mathbf{d}}^{\mathrm{T}}\tilde{\mathbf{d}}$. Based on this property, the CBF h_j is modified to provide robustness against the disturbance estimation error $\tilde{\mathbf{d}}$

$$h_j^d = h_j - c_2 V_d \tag{37}$$

where $c_2 > 0$, then define the following new set:

$$C_j^d = \left\{\mathbf{p} \in \mathbb{R}^3 : h_j^d \ge 0\right\} \tag{38}$$

From $V_d \ge 0$, it follows that $C_j^d \subseteq C_j$. Therefore, if C_j^d is forward invariant with respect to the UAV system (3), then C_j is also forward invariant.

Theorem 3. Consider the fixed-wing UAV system (3), the PTDO (18)-(20), and the composite controller $\mathbf{u} = \bar{\mathbf{u}} - m\mathbf{R}^{-1}\hat{\mathbf{d}}$. If $\bar{\mathbf{u}}$ satisfies the following condition

$$\frac{\mathbf{n}_j^{\mathrm{T}}\mathbf{R}\bar{\mathbf{u}}}{m} + Q_j - \frac{\gamma T_c \mathbf{n}_j^{\mathrm{T}}\mathbf{n}_j}{4c_2\pi - 2\gamma T_c c_2 c_3} \ge -c_3 h_j \tag{39}$$

where $c_3 > 0$, $2\pi - \gamma T_c c_3 > 0$, $\mathbf{n}_j = \boldsymbol{\delta}_j / \| \boldsymbol{\delta}_j \|$, and $Q_j = \mathbf{n}_j^{\mathrm{T}}\left(\boldsymbol{\alpha} - \ddot{\mathbf{p}}_j\right) + \| \dot{\boldsymbol{\delta}}_j \|^2 / \| \boldsymbol{\delta}_j \| - \left(\boldsymbol{\delta}_j^{\mathrm{T}} \dot{\boldsymbol{\delta}}_j\right)^2 / \| \boldsymbol{\delta}_j \|^3 + c_1 \mathbf{n}_j^{\mathrm{T}} \dot{\boldsymbol{\delta}}_j$, then the set S_j is forward invariant with respect to UAV system (3), implying that the UAV can achieve collision avoidance.

Proof. Taking the derivative of h_j^d and substituting $\mathbf{u} = \bar{\mathbf{u}} - m\mathbf{R}^{-1}\hat{\mathbf{d}}$ yields:

$$\begin{aligned} \dot{h}_j^d &= \ddot{\rho}_j + c_1 \dot{\rho}_j - c_2 \dot{V}_d \\ &= \mathbf{n}_j^{\mathrm{T}}\left(\frac{\mathbf{R}}{m}\left(\bar{\mathbf{u}} - m\mathbf{R}^{-1}\hat{\mathbf{d}}\right) + \boldsymbol{\alpha} + \mathbf{d} - \ddot{\mathbf{p}}_j\right) \\ &\quad + \frac{\| \dot{\boldsymbol{\delta}}_j \|^2}{\| \boldsymbol{\delta}_j \|} - \frac{\left(\boldsymbol{\delta}_j^{\mathrm{T}}\dot{\boldsymbol{\delta}}_j\right)^2}{\| \boldsymbol{\delta}_j \|^3} + c_1 \mathbf{n}_j^{\mathrm{T}} \dot{\boldsymbol{\delta}}_j - c_2 \dot{V}_d \\ &= \frac{\mathbf{n}_j^{\mathrm{T}}\mathbf{R}\bar{\mathbf{u}}}{m} + Q_j + \mathbf{n}_j^{\mathrm{T}}\tilde{\mathbf{d}} - c_2 \dot{V}_d \end{aligned} \tag{40}$$

From Eqs. (23) and (24), it follows that

$$\dot{V}_d \le -\frac{\pi}{\gamma T_c}\left(\beta^{\gamma} V_d^{1-\frac{\gamma}{2}} + \beta^{-\gamma} V_d^{1+\frac{\gamma}{2}}\right) \tag{41}$$

Substituting Eq. (41) into Eq. (40) yields

$$\begin{aligned} \dot{h}_j^d &\ge \frac{\mathbf{n}_j^{\mathrm{T}}\mathbf{R}\bar{\mathbf{u}}}{m} + Q_j + \mathbf{n}_j^{\mathrm{T}}\tilde{\mathbf{d}} + \frac{\pi c_2}{\gamma T_c}\left(\beta^{\gamma} V_d^{1-\frac{\gamma}{2}} + \beta^{-\gamma} V_d^{1+\frac{\gamma}{2}}\right) \\ &\ge \frac{\mathbf{n}_j^{\mathrm{T}}\mathbf{R}\bar{\mathbf{u}}}{m} + Q_j + \mathbf{n}_j^{\mathrm{T}}\tilde{\mathbf{d}} + \frac{2\pi c_2}{\gamma T_c} V_d \\ &= \frac{\mathbf{n}_j^{\mathrm{T}}\mathbf{R}\bar{\mathbf{u}}}{m} + Q_j + \mathbf{n}_j^{\mathrm{T}}\tilde{\mathbf{d}} + \frac{\pi c_2}{\gamma T_c}\tilde{\mathbf{d}}^{\mathrm{T}}\tilde{\mathbf{d}} - \frac{c_2 c_3}{2}\tilde{\mathbf{d}}^{\mathrm{T}}\tilde{\mathbf{d}} + \frac{c_2 c_3}{2}\tilde{\mathbf{d}}^{\mathrm{T}}\tilde{\mathbf{d}} \end{aligned} \tag{42}$$

Since

$$\begin{aligned} &\mathbf{n}_j^{\mathrm{T}}\tilde{\mathbf{d}} + \left(\frac{\pi c_2}{\gamma T_c} - \frac{c_2 c_3}{2}\right)\tilde{\mathbf{d}}^{\mathrm{T}}\tilde{\mathbf{d}} \\ &= -\frac{\gamma T_c \mathbf{n}_j^{\mathrm{T}}\mathbf{n}_j}{4c_2\pi - 2\gamma T_c c_2 c_3} \\ &\quad + \sum_{k}^{\{x,y,z\}}\left(\sqrt{\frac{\pi c_2}{\gamma T_c} - \frac{c_2 c_3}{2}}\tilde{d}_k + \frac{\sqrt{\gamma T_c}}{\sqrt{4c_2\pi - 2\gamma T_c c_2 c_3}} n_{j,k}\right)^2 \end{aligned} \tag{43}$$

it follows that:

$$\dot{h}_j^d \ge \frac{\mathbf{n}_j^{\mathrm{T}}\mathbf{R}\bar{\mathbf{u}}}{m} + Q_j - \frac{\gamma T_c \mathbf{n}_j^{\mathrm{T}}\mathbf{n}_j}{4c_2\pi - 2\gamma T_c c_2 c_3} + \frac{c_2 c_3}{2}\tilde{\mathbf{d}}^{\mathrm{T}}\tilde{\mathbf{d}} \tag{44}$$

Substituting Eq. (39) into Eq. (44) leads to:

$$\dot{h}_j^d \ge -c_3 h_j + \frac{c_2 c_3}{2}\tilde{\mathbf{d}}^{\mathrm{T}}\tilde{\mathbf{d}} = -c_3 h_j^d \tag{45}$$

From Eq. (45) and Definition 2, it can be concluded that h_j^d is a CBF for system (3) on the set C_j^d. Therefore, by Lemma 1, if the initial state satisfies $h_j^d(0) > 0$, then $h_j^d(t) \ge 0$ for all $t \ge 0$. Since $C_j^d \subseteq C_j$, it also holds that $h_j(t) \ge 0$ for all $t \ge 0$, implying that $\dot{\rho}_j(t) + c_1\rho_j(t) \ge 0$ for all $t \ge 0$. Hence, it follows that $\rho_j(t) \ge \rho_j(0)\exp(-c_1 t)$. When $\rho_j(0) \in S_j$, it holds that $\rho_j(t) \ge 0$ for all $t \ge 0$. In conclusion, the set S_j is forward invariant with respect to the UAV system (3). Thus, as long as the inequality constraint (39) is satisfied, the UAV achieves collision avoidance. This completes the proof of Theorem 3.

Remark 5. In Theorem 3, suppose that $h_j^d(0) > 0$, where $h_j^d = h_j - c_2 V_d$ and $V_d = \frac{1}{2}\widetilde{\mathbf{d}}^{\mathrm{T}}\widetilde{\mathbf{d}}$. Initially, the estimation error $\widetilde{\mathbf{d}}$ is relatively large, which results in conservatism of the proposed control scheme. However, as time approaches T_c, the estimation error $\widetilde{\mathbf{d}}$converges to zero, and the influence of disturbances on safety vanishes, thereby reducing the conservatism of the proposed method. Moreover, the condition $2\pi - \gamma T_c c_3 > 0$ implies that the disturbance observer dynamics characterized by $\frac{2\pi}{\gamma T_c}$ must converge faster than the exponential rate c_3 associated with the CBF constraint.

Remark 6. In [45–47], safety control methods based on disturbance observers are considered, where the CBF constraints depend on the upper bound of the disturbance estimation error $\widetilde{\mathbf{d}}$. The method in [48] guarantees $C_j^d = C_j$ only asymptotically as time tends to infinity, which is unsuitable for tasks requiring fast response, such as dynamic obstacle avoidance. In contrast, the safety condition (39) proposed in this paper does not explicitly depend on the estimation error $\widetilde{\mathbf{d}}$, thereby providing greater design flexibility. Moreover, benefiting from the PTDO, when $t \geq T_c$, it holds that $C_j^d = C_j$, which eliminates the effect of disturbances on system safety within the predefined time.

5.2. Safety-Critical Controller

By integrating the PPC-based controller (33) with the collision avoidance condition (39) within a QP framework, the controller (33) is preserved when the collision avoidance condition is satisfied; otherwise, it is modified minimally, as detailed below:

$$\begin{aligned} &\bar{\mathbf{u}}^* = \underset{\bar{\mathbf{u}}\in\mathbb{R}^m}{\operatorname{argmin}} \parallel \bar{\mathbf{u}} - \mathbf{u}_d - m\mathbf{R}^{-1}\widehat{\mathbf{d}} \parallel \\ &\text{s.t.} \frac{\mathbf{n}_j^{\mathrm{T}}\mathbf{R}\bar{\mathbf{u}}}{m} \geq -c_3 h_j - Q_j + \frac{\gamma T_c \mathbf{n}_j^{\mathrm{T}}\mathbf{n}_j}{4c_2\pi - 2\gamma T_c c_2 c_3}, j = 1, \ldots, M \end{aligned} \tag{46}$$

where $\mathbf{u}_d$ is defined in Eq. (33). Then, the safe control input for the UAV is given by:

$$\mathbf{u}_s = \bar{\mathbf{u}}^* - m\mathbf{R}^{-1}\widehat{\mathbf{d}} \tag{47}$$

In this paper, the collision-free conditions are treated as hard constraints, whereas the prescribed performance requirements are regarded as soft constraints. By formulating the QP problem (46), a trade-off between safety and performance is achieved. When obstacle avoidance is not required, the safe control input $\mathbf{u}_s$ coincides with the nominal control input $\mathbf{u}_d$, thus ensuring the prescribed performance requirements are fully satisfied. Conversely, when the obstacle avoidance mechanism is activated, only minimal modification is applied to $\mathbf{u}_d$. To quantify the impact of obstacle avoidance on system performance, nonnegative adaptive adjustment signals $\lambda_{1,u}$ and $\lambda_{1,l}$ are introduced to dynamically adjust the performance boundaries. Consequently, the system is able to maximally approximate the original performance requirements while guaranteeing safety.

Remark 7. If the input saturation constraints of the UAV are further considered, i.e., $\mathbf{u}_{\min} \leq \mathbf{u} \leq \mathbf{u}_{\max}$, this physical limitation can be incorporated into the optimization problem, leading to the following extended formulation:

$$\begin{aligned} &\bar{\mathbf{u}}^* = \operatorname{argmin} \parallel \bar{\mathbf{u}} - \mathbf{u}_d - m\mathbf{R}^{-1}\widehat{\mathbf{d}} \parallel \\ &\text{s.t.} \frac{\mathbf{n}_j^{\mathrm{T}}\mathbf{R}\bar{\mathbf{u}}}{m} \geq -c_3 h_j - Q_j + \frac{\gamma T_c \mathbf{n}_j^{\mathrm{T}}\mathbf{n}_j}{4c_2\pi - 2\gamma T_c c_2 c_3}, j = 1, \ldots, M \\ &\bar{\mathbf{u}} \geq \mathbf{u}_{\min} + m\mathbf{R}^{-1}\widehat{\mathbf{d}} \\ &\bar{\mathbf{u}} \leq \mathbf{u}_{\max} + m\mathbf{R}^{-1}\widehat{\mathbf{d}} \end{aligned} \tag{48}$$

By solving the above optimization problem (48), the safe control input $\mathbf{u}_s$ not only satisfies the collision avoidance conditions but also strictly adheres to the input saturation constraints. Moreover, since the input to the auxiliary system (18) is defined as the deviation between the nominal and safe control input, the nonnegative adaptive adjustment signals $\lambda_{1,u}$ and $\lambda_{1,l}$ can quantify the performance degradation caused by obstacle avoidance and input saturation. Despite the incorporation of this additional constraint, the proposed control scheme maintains stable system operation.

6. Simulation Results

This section validates the effectiveness of the proposed control scheme and the correctness of the theoretical analysis through numerical simulations. In the simulation, a fixed-wing UAV is tasked with tracking the following desired trajectory:

$$\mathbf{p}_d(t) = [100\cos(0.2t), 100\sin(0.2t), 2t]^{\mathrm{T}}\mathrm{m}$$

The flight environment is assumed to contain $M = 2$ spherical obstacles: one static obstacle fixed at:

$$\mathbf{p}_1 = [100\cos(8), 100\sin(8), 80]^{\mathrm{T}}\mathrm{m}$$

and one dynamic obstacle whose motion trajectory is defined as:

$$\mathbf{p}_2(t) = \begin{bmatrix} 100\cos(4) \\ 100\sin(4) \\ 40 \end{bmatrix} + \frac{t-20}{40}\begin{bmatrix} 100(\cos(12)-\cos(4)) \\ 100(\sin(12)-\sin(4)) \\ 80 \end{bmatrix}\mathrm{m}.$$

Both obstacles are modeled as spheres with a radius of $r_j = 10\mathrm{m}. j = 1,2$. Therefore, the UAV must execute effective obstacle avoidance maneuvers in the vicinity of $\mathbf{p}_1$ and $\mathbf{p}_2(t)$ to ensure flight safety.

The UAV mass is set to $m = 5\mathrm{kg}$, and the minimum safe distance for obstacle avoidance is specified as $r_s = 10\mathrm{m}$. By considering engineering practice, the lower and upper bounds of the control input $\mathbf{u}$ are denoted by $\mathbf{u}_{\max} = [200, 150, 100]^{\mathrm{T}}\mathrm{N}$ and $\mathbf{u}_{\min} = [20, -150, -100]^{\mathrm{T}}\mathrm{N}$, respectively.

To evaluate the robustness of the proposed control method and demonstrate the effectiveness of the PTDO, a set of unknown disturbances is introduced into the UAV system during the simulation. These disturbances are specified as follows: $d_x = 4\sin(0.1t)$, $d_y = 3\sin(0.1t) - \cos(0.3t)$, $d_z = -5\cos(-0.5t)$, $d_V = 2\cos(0.1t)$, $d_\theta = 0.8\cos(0.2t)$, $d_\psi = 0.5\sin(0.1t)$.

The user-specified convergence time for the tracking error $e_i(t), i = x, y, z$ is set to 10s, and the steady-state error tolerance is set to 0.1m. Accordingly, the parameters of the PPFs (12) and (13) are selected as $t_{i,f} = 10$ and $\eta_{i,f} = 0.1$. In addition, suitable parameters $\overline{\eta}_{i,0} = \underline{\eta}_{i,0} = 2$ are chosen to compress the error evolution space, thereby ensuring a small overshoot. The parameters of the auxiliary system (18) are chosen as $\mathrm{M}_1 = 0.8\mathbf{I}_3$ and $\mathrm{M}_2 = 0.8\mathbf{I}_3$. The PTDO parameters are selected as $\gamma = 0.3$ and $T_c = 2$, while the parameters of the prescribed performance trajectory tracking controller are specified as $g_1 = 4$ and $g_2 = 5$. The corresponding CBF parameters are chosen as $c_1 = 1$, $c_2 = 0.1$ and $c_3 = 1$. It is verified that the selected parameters satisfy the condition: $2\pi - \gamma T_c c_3 > 0$.

To verify the effectiveness of the proposed control scheme under different initial tracking errors, three cases with distinct initial positions are considered: Case 1: $\mathbf{p}(0) = [50, 10, 0]^{\mathrm{T}}\mathrm{m}$; Case 2: $\mathbf{p}(0) = [30, -20, -15]^{\mathrm{T}}\mathrm{m}$; Case 3: $\mathbf{p}(0) = [120, 30, 10]^{\mathrm{T}}\mathrm{m}$. The actual flight trajectories of the UAV for these cases are illustrated in Fig. 5. As shown in the figure, under all initial positions, the UAV successfully avoids both static and dynamic obstacles in the environment and accomplishes the desired trajectory tracking task. It is worth noting that, since the initial tracking error is explicitly considered in the design of the performance function, manual tuning of the design parameters is unnecessary, even

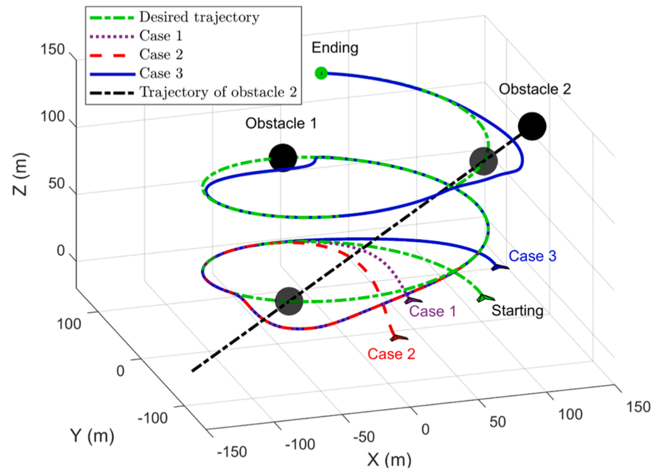

Fig. 5. Trajectory tracking results under different initial conditions.

when the initial position of the UAV changes.

Taking Case 3 as an example, Figs. 6, 7, 8, 9, 10 present the simulation results of UAV trajectory tracking with obstacle avoidance. The time evolution of the trajectory tracking error $e_i(t), i = x, y, z$ is depicted in Fig. 6, while Fig. 7 shows the time responses of the adaptive adjustment signals $\lambda_{1,u}$ and $\lambda_{1,l}$. When obstacle avoidance is not required, the tracking error converges to a steady-state accuracy of 0.1m within the user-specified convergence time of 10s, with only a small overshoot. When obstacle avoidance is necessary, $\lambda_{1,u}$ and $\lambda_{1,l}$ relax the performance boundaries, allowing for tolerable performance degradation induced by obstacle avoidance. Once the avoidance maneuver is completed, the adaptive adjustment signals converge to zero, thereby restoring the original performance constraints.

Fig. 8 demonstrates the estimation performance of the PTDO. The proposed PTDO can accurately estimate the total disturbance $\mathbf{d}$ within the prescribed time $T_c = 2$s. The safety-related variables ρ_j, h_j and h_j^d with $j = 1, 2$ are shown in Fig. 9. It can be observed that when $t \geq T_c$, $h_j^d = h_j$, indicating that the influence of disturbances on system safety is completely eliminated. Moreover, $\rho_j(t) \geq 0$ holds for all $t \geq 0$, demonstrating that the UAV successfully avoids collisions throughout the flight. Fig. 10 presents the actual control input $\mathbf{u}_s$ of the UAV. The input remains within the prescribed bounds, thereby confirming the effectiveness of the proposed control scheme under input constraints.

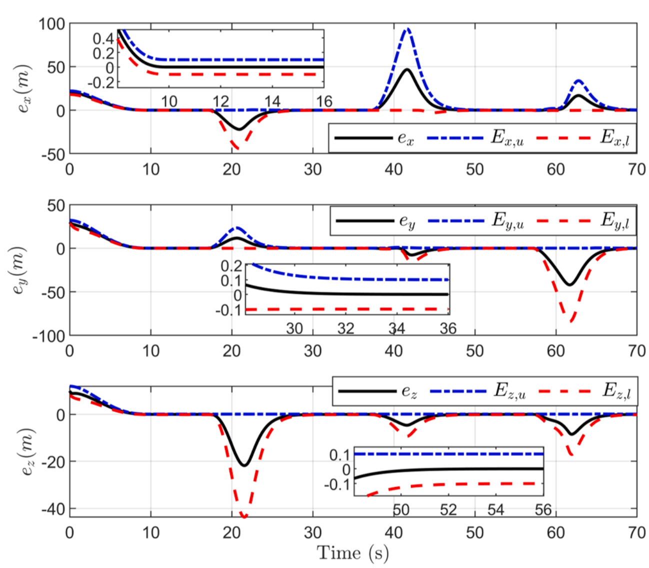

Fig. 6. Variation of tracking error with time in Case 3.

Owing to the novelty of the integrated control scheme combining PTDO, CBF, and PPC within a QP framework, directly comparable methods are scarcely available in the literature. Therefore, comprehensive comparisons are conducted against the individual components of the proposed framework to isolate and demonstrate the contribution of each part. To demonstrate the performance advantages of the PTDO, comparative simulations are conducted under identical initial conditions and disturbances, benchmarked against the fixed-time disturbance observers (FTDOs) in [9] and [52]. Fig. 11 illustrates the disturbance estimation error $\| \tilde{\mathbf{d}} \|$ over time for different observers. The results confirm that, compared with FTDOs, the PTDO provides faster convergence, improved estimation accuracy, and a predefined convergence time.

Furthermore, for comparison, safety constraints are formulated using the CBF from [32] and the RCBF from [44], respectively. The corresponding controllers (49) and (50) are then generated via QP, as formulated below:

$$\begin{aligned} &\mathbf{u}_s = \operatorname{argmin} \| \mathbf{u} - \mathbf{u}_d \| \\ &\text{s.t.} \frac{\mathbf{n}_j^{\mathrm{T}} \mathbf{R} \bar{\mathbf{u}}}{m} + Q_j \geq -c_3 h_j, j = 1, \ldots, M \\ &\mathbf{u}_{\min} \leq \mathbf{u} \leq \mathbf{u}_{\max} \end{aligned} \tag{49}$$

$$\begin{aligned} &\mathbf{u}_s = \operatorname{argmin} \| \mathbf{u} - \mathbf{u}_d \| \\ &\text{s.t.} \frac{\mathbf{n}_j^{\mathrm{T}} \mathbf{R} \bar{\mathbf{u}}}{m} + Q_j - \bar{d} \| \mathbf{n}_j \| \geq -c_3 h_j, j = 1, \ldots, M \\ &\mathbf{u}_{\min} \leq \mathbf{u} \leq \mathbf{u}_{\max} \end{aligned} \tag{50}$$

where $\mathbf{u}_d$ is defined in Eq. (33), and $\bar{d}$ satisfies $\| \mathbf{d} \| \leq \bar{d}$. The simulation setup remains consistent with Case 3, and the results are presented in Figs. 12–14. The results indicate that, under controller (49), $\rho_1 < 0$occurs at approximately $t = 41.5$s, indicating that UAV safety cannot be strictly guaranteed and that a collision may occur during flight. This is primarily because the effect of disturbances is not considered in the construction of the CBF. In contrast, when controller (50) is applied, UAV safety is effectively maintained. However, since the RCBF is designed based on the upper bound of the disturbance, the resulting distance between the UAV and the obstacle significantly exceeds the required safety margin, leading to a considerable trajectory tracking error. In comparison, the proposed CBF constructed using the PTDO preserves tracking performance to the greatest extent possible while ensuring flight safety.

7. Conclusions

Trajectory tracking for a fixed-wing UAV under performance constraints in environments with unknown disturbances and obstacles has been investigated in this paper. A safe trajectory-tracking control strategy under flexible performance constraints is proposed to preserve tracking performance as much as possible while ensuring safety. Theoretical analysis and simulation results demonstrate that the proposed method can strictly guarantee obstacle avoidance and accomplish the tracking task even in the presence of external disturbances, thereby achieving a favorable trade-off between safety and performance. However, two problems remain to be addressed. First, when the system is subject to input saturation, the QP problem may become infeasible. Second, current methods have only been tested in numerical simulations, which limits the demonstration of their practical engineering value. Therefore, future work will focus on ensuring the feasibility of QP problems under input constraints and validating the effectiveness of the proposed control scheme through hardware experiments.

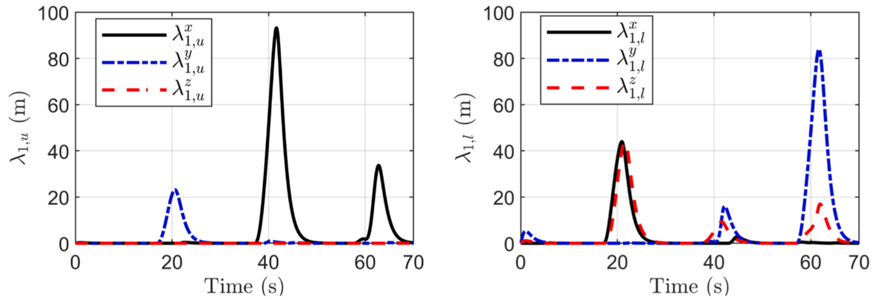

Fig. 7. Time evolution of the adaptive adjustment signals in Case 3.

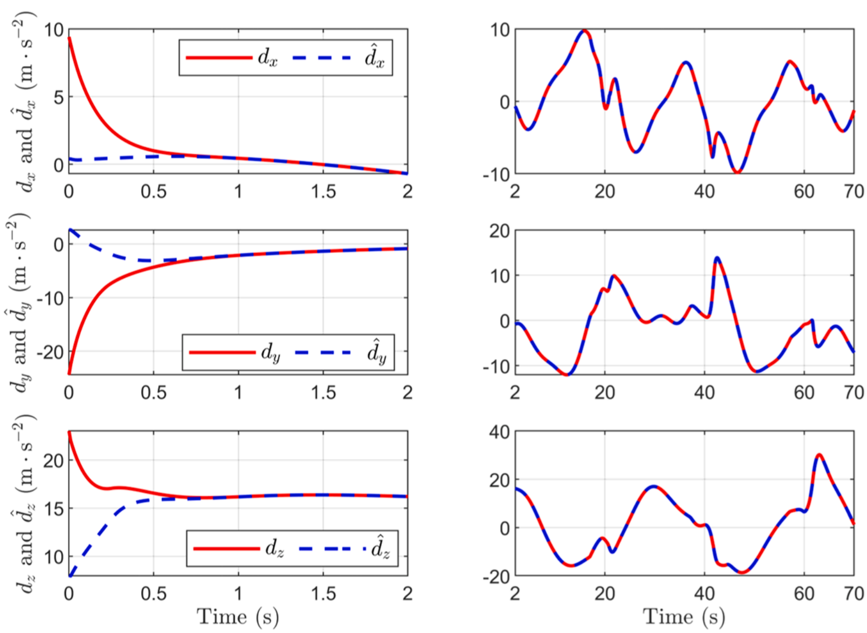

Fig. 8. Time evolution of the disturbance and its estimation in Case 3.

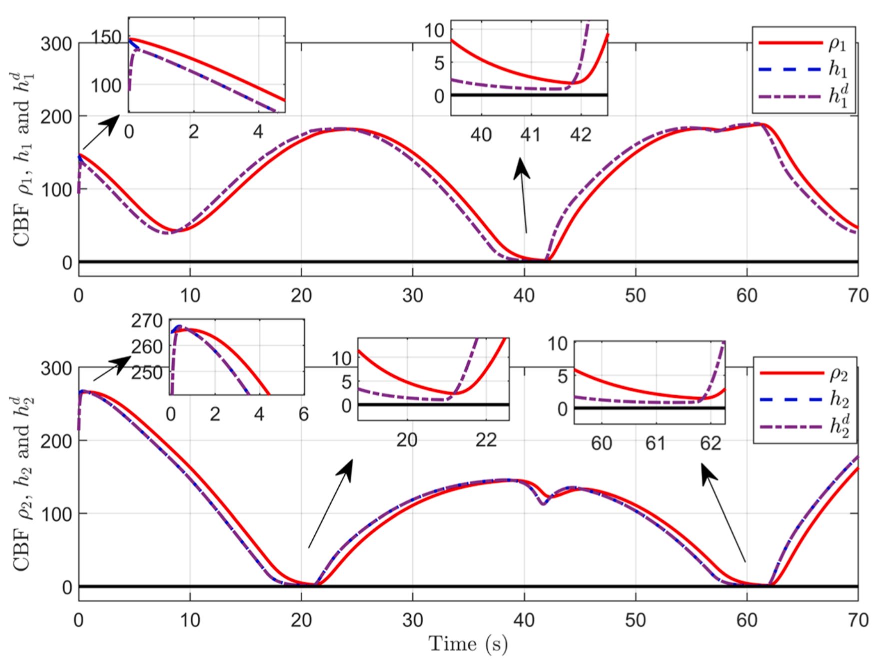

Fig. 9. Plot of safety-related variables in Case 3.

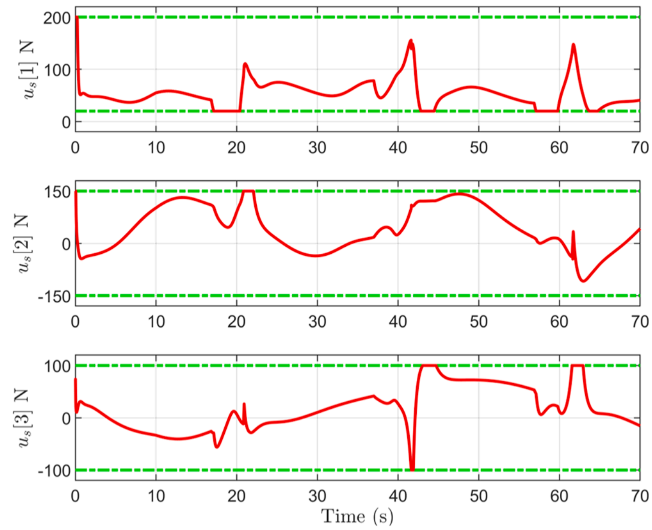

Fig. 10. Actual control input of the UAV in Case 3.

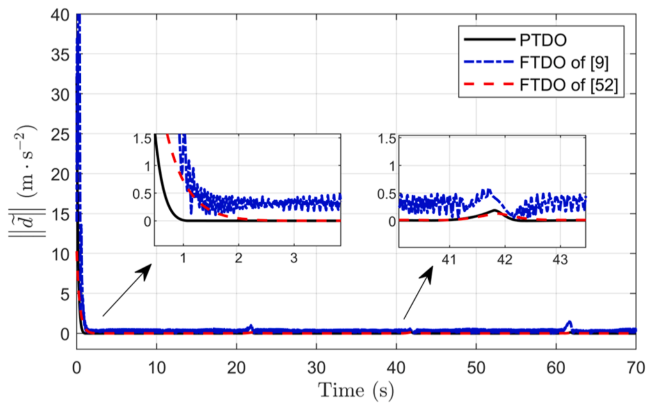

Fig. 11. Comparison of disturbance estimation errors over time for different observers.

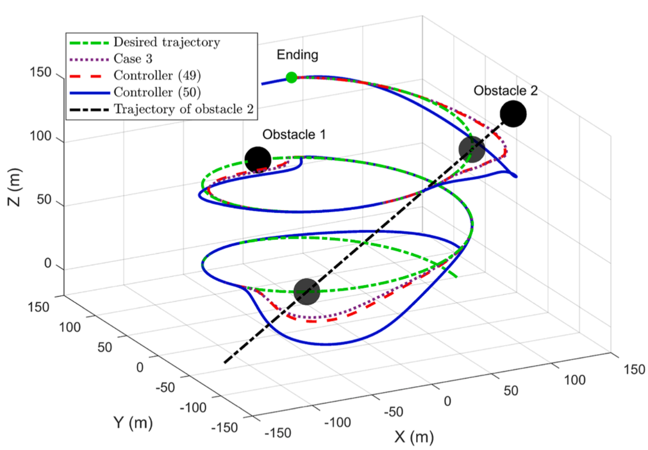

Fig. 12. Trajectory tracking results under different controllers.

CRediT authorship contribution statement

Chao Yan: Writing – review & editing, Writing – original draft, Validation, Formal analysis, Data curation, Conceptualization. **Zexu Zhang:** Supervision, Resources, Funding acquisition. **Weimin Bao:** Supervision, Funding acquisition. **Kai Zhang:** Writing – review & editing, Supervision, Methodology, Investigation. **Liang Zhang:** Writing – review & editing, Supervision.

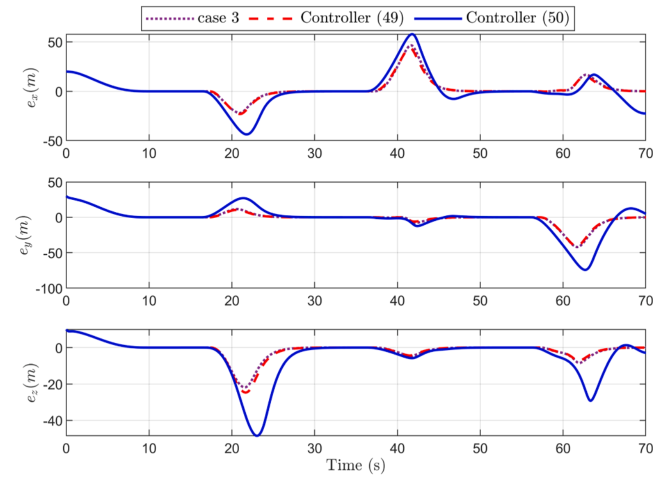

Fig. 13. UAV tracking errors under different controllers.

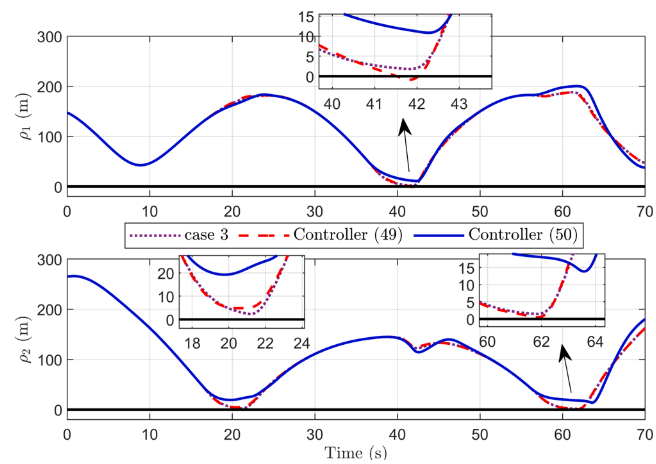

Fig. 14. Plot of variables$\rho_j(t), j = 1, 2$over time under different controllers.

Declaration of competing interest

The authors declare that they have no known competing financial interests or personal relationships that could have appeared to influence the work reported in this paper.

Acknowledgements

This work is supported by the Aeronautical Science Foundation of China (2024Z023077001), the National Natural Science Foundation of China (52238002, 62303002).

Data availability

No data was used for the research described in the article.

References

[1] H. Liu, S. Liu, Y. Tian, K. Sun, Hierarchical decision-making model for multi-aircraft formation in forest firefighting missions, Aerosp. Sci. Technol. 163 (2025) 110242.

[2] W. Yang, Distributed robust adaptive practical finite-time formation tracking control of fixed-wing UAVs, Aerosp. Sci. Technol. 166 (2025) 110552.

[3] S. Huang, J. Shi, Q. Zhu, Z. Du, Y. Lyu, Z. Liu, Multiple UAVs cooperatively circumnavigating a group of non-cooperative targets in a GPS-free environment via a range-only distributed controller, Aerosp. Sci. Technol. 158 (2025) 109924.
[4] A.P. Aguiar, J.P. Hespanha, Trajectory-tracking and path-following of underactuated autonomous vehicles with parametric modeling uncertainty, IEEE Trans. Autom. Control 52 (2007) 1362–1379.
[5] M. Lungu, Auto-landing of fixed wing unmanned aerial vehicles using the backstepping control, ISA Trans 95 (2019) 194–210.
[6] W. Yang, Z. Shi, Y. Zhong, Robust adaptive three-dimensional trajectory tracking control scheme design for small fixed-wing UAVs, ISA Trans 141 (2023) 377–391.
[7] J. Li, S. Chen, C. Li, C. Gao, W. Jing, Adaptive control of underactuated flight vehicles with moving mass, Aerosp. Sci. Technol. 85 (2019) 75–84.
[8] K.K. Zhang, B. Zhou, H. Jiang, G.R. Duan, Finite-time control of a class of nonlinear underactuated systems with application to underactuated axisymmetric spacecraft, IEEE Trans. Aerosp. Electron. Syst. 59 (2023) 7061–7071.
[9] S. Zhao, J. Zheng, F. Yi, X. Wang, Z. Zuo, Exponential predefined time trajectory tracking control for fixed-wing UAV with input saturation, IEEE Trans. Aerosp. Electron. Syst. 60 (2024) 6406–6419.
[10] C.P. Bechlioulis, G.A. Rovithakis, Robust adaptive control of feedback linearizable MIMO nonlinear systems with prescribed performance, IEEE Trans. Autom. Control 53 (2008) 2090–2099.
[11] J. Tan, S. Xue, H. Li, Z. Guo, H. Cao, B. Chen, Hierarchical Safe Reinforcement Learning Control for Leader-Follower Systems With Prescribed Performance, IEEE Trans. Autom. Sci. Eng. 22 (2025) 19568–19581.
[12] K. Yong, M. Chen, Y. Shi, Q. Wu, Flexible performance-based robust control for a class of nonlinear systems with input saturation, Automatica 122 (2020) 109268.
[13] K. Yong, M. Chen, Y. Shi, Q. Wu, Flexible performance-based control for nonlinear systems under strong external disturbances, IEEE Trans. Cybern. 54 (2022) 762–775.
[14] M. Liu, X. Shao, G. Ma, Appointed-time fault-tolerant attitude tracking control of spacecraft with double-level guaranteed performance bounds, Aerosp. Sci. Technol. 92 (2019) 337–346.
[15] G. Cui, W. Yang, J. Yu, Z. Li, C. Tao, Fixed-time prescribed performance adaptive trajectory tracking control for a QUAV, IEEE Trans. Circuits Syst. II Express Briefs 69 (2022) 494–498.
[16] J. Tan, Y. Dong, P. Shao, G. Qu, Anti-saturation adaptive fault-tolerant control with fixed-time prescribed performance for UAV under AOA asymmetric constraint, Aerosp. Sci. Technol. 120 (2022) 107264.
[17] M. Tian, N. Wang, Z. Wang, Z. Fu, F. Tao, Prescribed-time fault-tolerant tracking control for quadrotor UAV with guaranteed performance, Aerosp. Sci. Technol. 161 (2025) 110162.
[18] X. Bu, B. Jiang, H. Lei, Nonfragile quantitative prescribed performance control of waverider vehicles with actuator saturation, IEEE Trans. Aerosp. Electron. Syst. 58 (2022) 3538–3548.
[19] R. Ji, B. Yang, J. Ma, S.S. Ge, Saturation-tolerant prescribed control for a class of MIMO nonlinear systems, IEEE Trans. Cybern. 52 (2022) 13012–13026.
[20] R. Ji, S.S. Ge, D. Li, Saturation-tolerant prescribed control for nonlinear systems with unknown control directions and external disturbances, IEEE Trans. Cybern. 54 (2024) 877–889.
[21] Y. Shi, B. Yi, W. Xie, W. Zhang, Enhancing prescribed performance of tracking control using monotone tube boundaries, Automatica 159 (2024) 111304.
[22] L. Sun, K. Sun, X. Guo, J. Yuan, M. Zhu, Enhancing prescribed-time trajectory tracking control for a stratospheric airship with prescribed performance, Chin. J. Aeronaut. 38 (2025) 10329.
[23] Y. Wang, H. Wang, J. Zhu, Y. Liu, M. Zhang, Z. Su, Flexible prescribed performance-based approaching control for UAV aerial recovery under multiwind disturbances, Chin. J. Aeronaut. 38 (2025) 103282.
[24] S. Sui, C.L.P. Chen, S. Tong, A novel full errors fixed-time control for constraint nonlinear systems, IEEE Trans. Autom. Control 68 (2023) 2568–2575.
[25] K. Zhao, Y. Song, C.L.P. Chen, L. Chen, Adaptive asymptotic tracking with global performance for nonlinear systems with unknown control directions, IEEE Trans. Autom. Control 67 (2022) 1566–1573.
[26] L. Shen, H. Wang, H. Yue, Prescribed performance adaptive fuzzy control for affine nonlinear systems with state constraints, IEEE Trans. Fuzzy Syst. 30 (2022) 5351–5360.
[27] Z. Wang, X. Liu, W. Wang, Prescribed performance control with a standard second-order transient response for strict feedback affine nonlinear systems, Int. J. Syst. Sci. 52 (2021) 2677–2688.
[28] Z. Wang, X. Liu, W. Wang, Adaptive prescribed performance control with selected transient response for a class of nonlinear systems with uncertainties, Int. J. Adapt. Control Process. 36 (2022) 670–689.
[29] H. Zhang, J. Huo, Y. Huang, J. Cheng, X. Li, Perception-Aware-Based UAV Trajectory Planner via Generative Adversarial Self-Imitation Learning From Demonstrations, IEEE Internet Things J 12 (2025) 3248–3260.
[30] L. Chen, H. Duan, Collision-free formation-containment control for a group of UAVs with unknown disturbances, Aerosp. Sci. Technol. 126 (2022) 107618.
[31] J. Qi, J. Guo, M. Wang, C. Wu, Z. Ma, Formation tracking and obstacle avoidance for multiple quadrotors with static and dynamic obstacles, IEEE Robot. Autom. Lett. 7 (2022) 1713–1720.
[32] A.D. Ames, X. Xu, J.W. Grizzle, P. Tabuada, Control barrier function based quadratic programs for safety critical systems, IEEE Trans. Autom. Control 62 (2017) 3861–3876.
[33] W. Xiao, C. Belta, High-order control barrier functions, IEEE Trans. Autom. Control 67 (2022) 3655–3662.
[34] X. Tan, W.S. Cortez, D.V. Dimarogonas, High-order barrier functions: Robustness, safety, and performance-critical control, IEEE Trans. Autom. Control 67 (2022) 3021–3028.
[35] J. Li, S. Song, Prescribed-time collision-free trajectory tracking control for spacecraft with position-only measurements, IEEE Trans. Aerosp. Electron. Syst. 60 (2024) 4035–4043.
[36] A. Singletary, K. Klingebiel, J. Bourne, A. Browning, P. Tokumaru, A. Ames, Comparative analysis of control barrier functions and artificial potential fields for obstacle avoidance, in: 2021 IEEE/RSJ International Conference on Intelligent Robots and Systems, IEEE, 2021, pp. 8129–8136.
[37] Z. Zuo, C. Liu, Q. Han, J. Song, Unmanned aerial vehicles: Control methods and future challenges, IEEE/CAA J. Autom. Sinica 9 (2022) 601–614.
[38] J. Li, S. Chen, C. Li, F. Wang, Distributed game strategy for formation flying of multiple spacecraft with disturbance rejection, IEEE Trans. Aerosp. Electron. Syst. 57 (2020) 119–128.
[39] X. Gao, Y. Long, T. Li, X. Hu, C.L.P. Chen, F. Sun, Optimal Fuzzy Output Feedback Control for Dynamic Positioning of Vessels With Finite-Time Disturbance Rejection Under Thruster Saturations, IEEE Trans. Fuzzy Syst. 31 (2023) 3447–3458.
[40] S. Kolathaya, A.D. Ames, Input-to-state safety with control barrier functions, IEEE Control Syst. Lett. 3 (2019) 108–113.
[41] A. Alan, A.J. Taylor, C.R. He, G. Orosz, A.D. Ames, Safe controller synthesis with tunable input-to-state safe control barrier functions, IEEE Control Syst. Lett. 6 (2022) 908–913.
[42] J. Buch, S.C. Liao, P. Seiler, Robust control barrier functions with sector-bounded uncertainties, IEEE Control Syst. Lett. 6 (2022) 1994–1999.
[43] Q. Nguyen, K. Sreenath, Robust safety-critical control for dynamic robotics, IEEE Trans. Autom. Control 67 (2022) 1073–1088.
[44] B. An, H. Fan, B. Wang, L. Liu, Y. Wang, Velocity-constrained distributed formation tracking of fixed-wing UAVs with multiple leaders, Aerosp. Sci. Technol. 154 (2024) 109514.
[45] A. Alan, T.G. Molnar, E. Das, A.D. Ames, G. Orosz, Disturbance observers for robust safety-critical control with control barrier functions, IEEE Control Syst. Lett. 7 (2023) 1123–1128.
[46] A. Isaly, O.S. Patil, H.M. Sweatland, R.G. Sanfelice, W.E. Dixon, Adaptive Safety with a RISE-Based Disturbance Observer, IEEE Trans. Autom. Control 69 (2024) 4883–4890.
[47] E. Daş, J.W. Burdick, Robust control barrier functions using uncertainty estimation with application to mobile robots, IEEE Trans. Autom. Control 70 (2025) 4766–4773.
[48] J. Sun, J. Yang, Z. Zeng, Safety-critical control with control barrier function based on disturbance observer, IEEE Trans. Autom. Control 69 (2024) 4750–4756.
[49] R.W. Beard, T.W. McLain, Small Unmanned Aircraft: Theory and Practice, Princeton University Press, 2012.
[50] L. Farina, S. Rinaldi, Positive linear systems: Theory and applications, John Wiley & Sons, 2011.
[51] D. Ye, A. Zou, Z. Sun, Predefined-time predefined-bounded attitude tracking control for rigid spacecraft, IEEE Trans. Aerosp. Electron. Syst. 58 (2021) 464–472.
[52] K. Liu, R. Wang, S. Zheng, S. Dong, G. Sun, Fixed-time disturbance observer-based robust fault-tolerant tracking control for uncertain quadrotor UAV subject to input delay, Nonlinear Dyn 107 (2022) 2363–2390.